

Supporting Information for:

Tuning the redox profile of the 6,6'-biazulenic platform through functionalization along its molecular axis

*Shaun R. Kelsey,^a Georgii Griaznov,^a Andrew D. Spaeth,^a Daron E. Janzen,^b Justin T. Douglas,^c
Ward H. Thompson^a and Mikhail V. Barybin^{*, a}*

^a Department of Chemistry, University of Kansas, 1567 Irving Hill Road,
Lawrence, Kansas 66045, United States

^b Department of Chemistry and Biochemistry, St. Catherine University, St. Paul, MN
55105, USA

^c NMR Laboratory, Molecular Structures Group, University of Kansas, Lawrence, KS
66045, USA

* To whom correspondence should be addressed. E-mail: mbarybin@ku.edu
(M.V.B.)

Table of Contents

A. Synthetic procedures

A1. General Procedures, Starting Materials, and Equipment	S-4
A2. Synthesis of 1,1',3,3'-tetraethoxycarbonyl-6,6'-biazulene (1)	S-5
A3. Synthesis of 2,2'-dichloro-1,1',3,3'-tetraethoxycarbonyl-6,6'-biazulene (3a)	S-6
Scheme S1. Two alternative routes to 3a starting from 2-amino-6-bromo-1,3-diethoxycarbonylazulene	S-7
A4. Synthesis of 2-chloro-1,1',3,3'-tetraethoxycarbonyl-6,6'-biazulene (3b)	S-8

B. NMR spectra

Figure S1. ¹ H NMR (400 MHz, CDCl ₃) spectrum of 1	S-9
Figure S2. ¹ H NMR (500 MHz, CDCl ₃) spectrum of 3a	S-10
Figure S3. ¹³ C{ ¹ H} NMR (126 MHz, CDCl ₃) spectrum of 3a	S-11
Figure S4. HSQC NMR (600 MHz, CDCl ₃) spectrum of 3a	S-12
Figure S5. HMBC NMR (500 MHz, CDCl ₃) spectrum of 3a	S-13
Figure S6. 1,1-ADEQUATE NMR (600 MHz, CDCl ₃) spectrum of 3a	S-14
Figure S7. ¹ H NMR (500 MHz, CDCl ₃) spectrum of 3b	S-15
Figure S8. ¹³ C{ ¹ H} NMR (126 MHz, CDCl ₃) spectrum of 3b	S-16

C. Electronic absorption spectra

Figure S9. Electronic absorption spectrum of 1	S-17
Figure S10. Electronic absorption spectrum of 3a	S-17
Figure S11. Electronic absorption spectrum of 3b	S-18
Table S1. Summary of the UV vis data for compounds 1 , 3a , and 3b	S-18

D. Computational work

D1. Calculation Details	S-19
Table S2. Coordinates of 6,6'-biazulene used in generating the HOMO/LUMO plots in Fig. 1.	S-20
Table S3. Coordinates of 3a used to simulate the UV-vis spectrum in Figure S12.	S-21
Table S4. Transition wavelengths, oscillator strengths, and transition orbital amplitudes obtained from the TD-DFT/B3LYP/cc-pVDZ calculations.	S-23
Figure S12. Experimental vs. TD-DFT simulated electronic spectra of 3a	S-24

E. Electrochemistry

Figure S13. Cyclic voltammogram and scan rate dependence data for 1	S-25
Figure S14. Cyclic voltammogram and scan rate dependence data for 2b	S-25
Figure S15. Cyclic voltammogram and scan rate dependence data for 3a	S-26
Figure S16. Cyclic voltammogram and scan rate dependence data for 3b	S-26
Figure S17. Cyclic voltammogram for 1,3-diethoxycarbonylazulene	S-27
Figure S18. Cyclic voltammogram for 2-amino-1,3-diethoxycarbonylazulene	S-27
Figure S19. Cyclic voltammogram for 2-chloro-1,3-diethoxycarbonylazulene	S-28
Figure S20. Cyclic voltammogram for 2-isocyano-1,3-diethoxycarbonylazulene	S-28
Table S5. E _{1/2} potentials and σ _p parameters for Fig. 4	S-29
Table S6. E _{1/2} potentials and σ _p parameters for Fig. 5	S-29

F. X-ray crystallographic studies

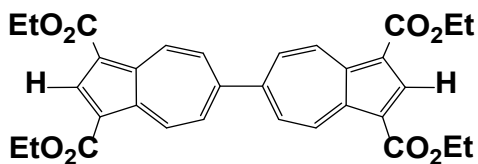
F1. Experimental and Refinement Model Description	S-30
Figure S21. Crystals of 3a	S-30
Table S7. Crystal data and structure refinement for 3a .	S-31
Table S8. Fractional Atomic Coordinates ($\times 10^4$) and Equivalent Isotropic Displacement Parameters ($\text{\AA}^2 \times 10^3$) for 3a .	S-32
Table S9. Anisotropic Displacement Parameters ($\text{\AA}^2 \times 10^3$) for 3a .	S-33
Table S10. Bond Lengths for 3a .	S-34
Table S11. Bond Angles for 3a .	S-35
Table S12. Torsion Angles for 3a .	S-36
Table S13. Hydrogen Atom Coordinates ($\text{\AA} \times 10^4$) and Isotropic Displacement Parameters ($\text{\AA}^2 \times 10^3$) for 3a .	S-37
Figure S22. Distribution of the C–Cl bond distances for chloroazulenes featuring Cl-substitution at the five-membered ring of their azulenic scaffold.	S-38
Table S14. X-ray crystallographically characterized chloroazulenes represented in Fig. 7.	S-38
Figure S23. The chlorodiphenylmethylium cation X-ray crystallographically characterized by Laube <i>et al.</i>	S-40
References	S-41

A. Synthetic procedures

A1. General Procedures, Starting Materials, and Equipment

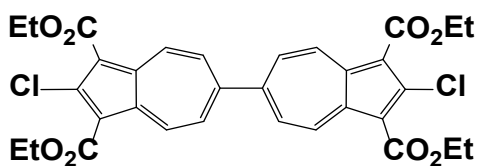
All synthetic operations were performed without protection from air. 2,2'-Diamino-1,1',3,3'-tetraethoxycarbonyl-6,6'-biazulene (**2a**),¹ 2-amino-1,1',3,3'-tetraethoxycarbonyl-6,6'-biazulene (**2b**),² 2,2'-diisocyano-1,1',3,3'-tetraethoxycarbonyl-6,6'-biazulene (**4a**),¹ 2-isocyano-1,1',3,3'-tetraethoxycarbonyl-6,6'-biazulene (**4b**),² 1,3-diethoxycarbonylazulene,³ 2-amino-1,3-diethoxycarbonylazulene,⁴ 2-chloro-1,3-diethoxycarbonylazulene,⁵ and 2-isocyano-1,3-diethoxycarbonylazulene⁶ were synthesized according to literature procedures. Other reagents and all solvents, including CDCl₃, were obtained from commercial sources and used as received. Infrared spectra were recorded on a PerkinElmer Spectrum 100 FTIR spectrometer with liquid samples sealed in 0.1 mm NaCl cells. NMR samples were analyzed on Bruker Avance III HD 400 MHz, Avance III 500 MHz, or Bruker AVIII 600 MHz spectrometers. ¹H and ¹³C NMR chemical shifts are given with reference to residual solvent resonances relative to SiMe₄. Electronic spectra were recorded at 22±3 °C using a Shimadzu UV-3600 UV-Vis-NIR spectrophotometer or a Varian Cary 50 Bio spectrophotometer. Cyclic voltammetry experiments were conducted at room temperature using an EPSILON (Bioanalytical Systems Inc., West Lafayette, IN) electrochemical workstation inside a Vacuum Atmospheres dry box filled with argon. A solution of 0.1 M [ⁿBu₄N][PF₆] in CH₂Cl₂ was used as the supporting electrolyte. A three-component system consisting of a glassy carbon working electrode, a platinum-wire auxiliary electrode, and a glass encased non-aqueous Ag/AgCl reference electrode was employed. The reported potentials were determined at a scan rate of 100 mV/s. Melting points are uncorrected and were determined for samples in sealed capillary tubes. Elemental analyses were carried out by Micro-Analysis, Inc., Wilmington, Delaware.

A2. Synthesis of 1,1',3,3'-tetraethoxycarbonyl-6,6'-biazulene (1)

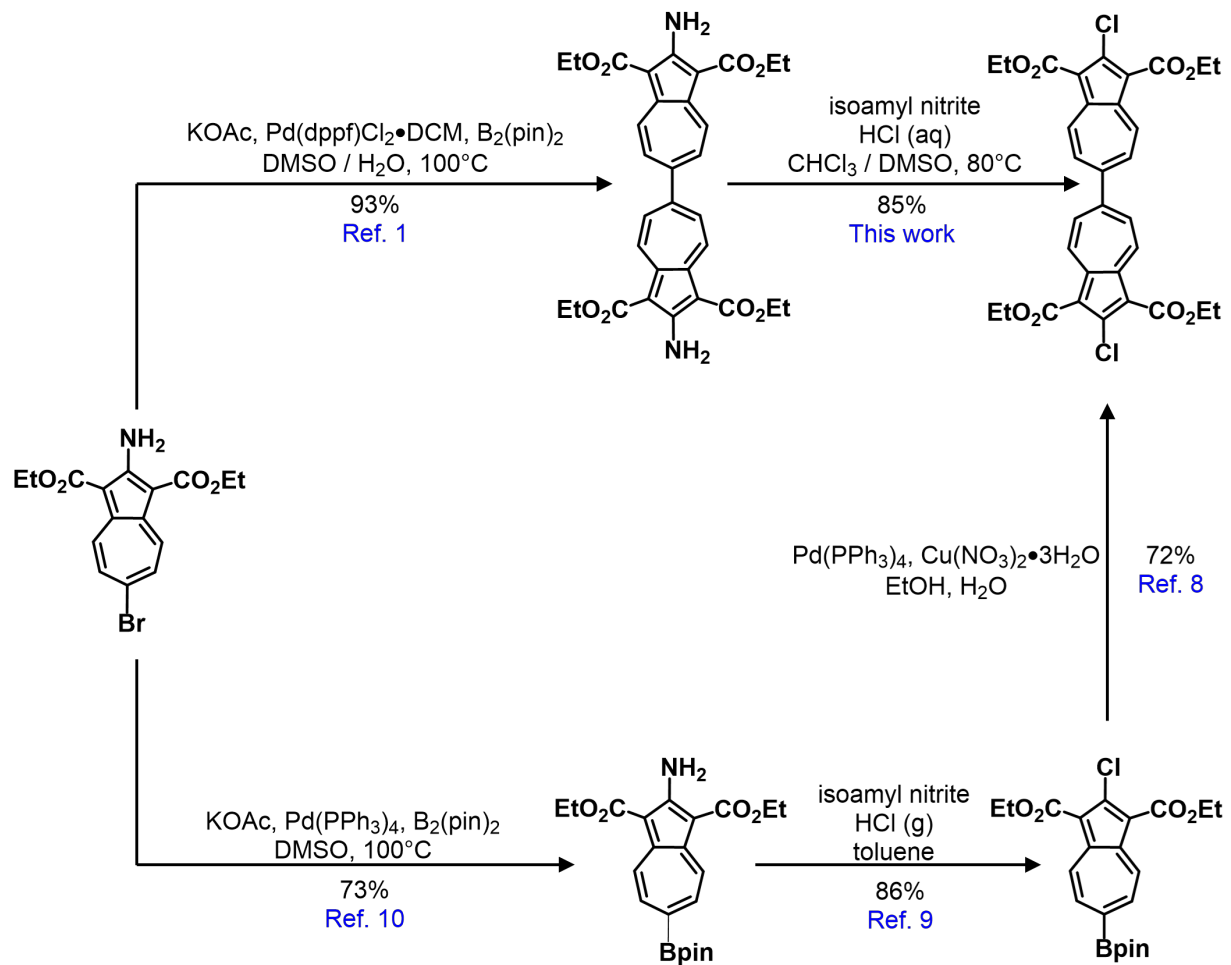


A solution composed of concentrated H_2SO_4 (98%, 0.173 g), 10 mL of THF and 50 mL of 1,4-dioxane was added to a mixture of **2a** (0.200 g, 0.349 mmol) and *para*-hydroxyquinone (0.077 g, 0.699 mmol) with stirring. To the resulting reaction mixture, a solution of isoamyl nitrite (1.88 mL, 14.0 mmol) in 35 mL of 1,4-dioxane and a solution of *para*-hydroxyquinone (1.54 g, 14.0 mmol) in 35 mL of 1,4-dioxane were added dropwise under vigorous stirring using separate addition funnels. Once the addition was completed, the mixture was stirred for 3 hours and then quenched with 200 mL of 1M aqueous Na_2SO_3 . After extraction with CH_2Cl_2 , the combined organic layers were washed with deionized H_2O (3×200 mL) and dried over anhydrous Na_2SO_4 . The drying agent was filtered off and the filtrate was concentrated to dryness under vacuum to afford a residue that was redissolved in a minimum amount of CH_2Cl_2 . The resulting solution was layered with pentane and kept at -40 °C until a red-brown precipitate formed. The solid was filtered off and dried at 10^{-2} torr to give **1** (0.096 g, 0.177 mmol) in a 51% yield. Mp: 175 °C (dec.) [lit. 227.5-230 °C⁷]. The NMR and UV-vis spectroscopic signatures of this product were identical to those of bona fide **1** previously reported⁷ by Ito *et al.* ¹H NMR (CDCl_3 , 400 MHz, 22 °C): δ 9.89 (d, 4H, $\text{H}^{4,4',8,8'}$, $^3J_{\text{HH}} = 11$ Hz), 8.92 (s, 2H, $\text{H}^{2,2'}$), 7.97 (d, 4H, $\text{H}^{5,5',7,7'}$, $^3J_{\text{HH}} = 11$ Hz), 4.48 (d, 8H, CH_2 , $^3J_{\text{HH}} = 7$ Hz), 1.49 (t, 12H, CH_3 , $^3J_{\text{HH}} = 7$ Hz), ppm. ¹³C {¹H} NMR (CDCl_3 , 126 MHz, 22 °C): δ 165.0 (C=O), 156.0, 144.6, 143.1, 138.6, 131.4, 117.5 (aromatic C), 60.5 (CH_2), 14.7 (CH_3) ppm. UV-Vis [CH_2Cl_2 , λ_{max} ($\epsilon \times 10^{-3} \text{ M}^{-1} \text{ cm}^{-1}$): 342 (63.58), 373 (47.06), 518 (2.24) nm.

A3. Synthesis of 2,2'-dichloro-1,1',3,3'-tetraethoxycarbonyl-6,6'-biazulene (**3a**)

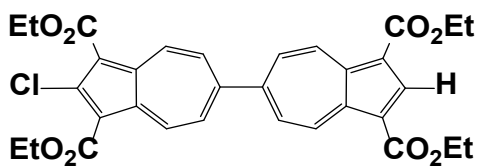


A red slurry consisting of **2a** (0.121 g, 0.211 mmol) and 12 M aqueous HCl (7 mL) was stirred at 22 °C for 15 minutes, then diluted with 7 mL of CHCl₃. The biphasic red mixture was stirred for an additional 5 minutes before it was treated with isoamyl nitrite (0.14 mL, 1.0 mmol) in one portion. The reaction mixture was stirred for an additional 15 minutes, during which time it quickly darkened and turned into a dark slurry. Then, DMSO (15 mL) was added, and the reaction flask was equipped with a reflux condenser. The temperature was raised to 80 °C, and the opaque solution slowly turned dark red/purple as it was stirred for an hour and 45 minutes. After this time, deionized water (100 mL) was added, and the product was extracted with CHCl₃ (4 × 30 mL). The combined organic extracts were washed with deionized water (6×30 mL) and dried over anhydrous Na₂SO₄. The drying agent was filtered off and the filtrate was concentrated to dryness under reduced pressure to afford **3a** (0.110 g, 0.179 mmol) in an 85% yield. Further recrystallization of the product from CH₂Cl₂/pentane provided large metallic black crystals of **3a** (Figure S21a). Mp: 220-222 °C, [lit. 222-224 °C⁸]. Anal. Calcd for C₃₂H₂₈Cl₂O₈: C, 62.86; H, 4.62; Found: C, 62.98; H, 4.84. ¹H NMR (400 MHz, CDCl₃): δ 9.60 (d, ³J_{HH} = 11.2 Hz, 4H, H^{4,4',8,8'}), 7.93 (d, ³J_{HH} = 11.2 Hz, 4H, H^{5,5',7,7'}), 4.52 (q, ³J_{HH} = 7.1 Hz, 8H, CH₂), 1.50 (t, ³J_{HH} = 7.1 Hz, 12H, CH₃) ppm. ¹³C{¹H} NMR (126 MHz, CDCl₃): δ 164.26 (C=O), 155.05 (C^{6,6'}), 144.78 (C^{2,2'}), 140.87 (C^{9,9',10,10'}), 137.27 (C^{4,4',8,8'}), 131.81 (C^{5,5',7,7'}), 116.56 (C^{1,1',3,3'}), 61.06 (CH₂), 14.57 (CH₃) ppm. UV-Vis [CH₂Cl₂, λ_{max} (ε × 10⁻³ M⁻¹ cm⁻¹): 340 (48.81), 368 (32.22), 396 (18.08), *ca.* 440-640 (1.06) nm.



Scheme S1. Two alternative routes to **3a** starting from 2-amino-6-bromo-1,3-diethoxycarbonylazulene.^{1, 8-10}

A4. Synthesis of 2-chloro-1,1',3,3'-tetraethoxycarbonyl-6,6'-biazulene (**3b**)



A biphasic mixture consisting of 12 M aqueous HCl (8 mL), **2b** (0.174 g, 0.312 mmol), and CHCl₃ (2 mL) was stirred for 10 minutes at 30 °C. Then isoamyl nitrite (0.17 mL, 1.27 mmol) was added in one portion followed by an additional 6 mL of CHCl₃. As the solution darkened, the reaction flask was equipped with a reflux condenser to prevent evaporation of CHCl₃. The heating was removed, and the color of the mixture gained a purple hue over a period of 4.5 hours. The temperature of the mixture was then raised to 60 °C for 19 hours. Deionized water (50 mL) was added, and the organic layer was separated and washed with deionized water (4 × 20 mL). The resulting solution was treated with 7.3 g of NaHCO₃. Sodium bicarbonate was filtered off, and the filtrate was dried over anhydrous Na₂SO₄. The drying agent was filtered off and the filtrate was concentrated to dryness under reduced pressure to afford dark red **3b** (0.158 g, 0.274 mmol) in an 88% yield. Mp: 180 °C (dec.). HRMS (m/z, ES⁺): Calcd for C₃₂H₂₉ClO₈⁺: 576.1551, found: 576.1578. ¹H NMR (500 MHz, CDCl₃): δ 9.88 (d, ³J_{HH} = 10.7 Hz, 2H, H^{4',8'}), 9.61 (d, ³J_{HH} = 10.7 Hz, 2H, H^{4,8}), 8.91 (s, 1H, H^{2'}), 7.94 (d, ³J_{HH} = 10.7 Hz, 4H, H^{5,5',7,7'}), 4.52 (q, ³J_{HH} = 7.1 Hz, 4H, CH₂), 4.47 (q, J = 7.1 Hz, 4H, CH₂), 1.50 (t, J = 7.2 Hz, 6H, CH₃), 1.47 (t, J = 7.2 Hz, 6H, CH₃) ppm. ¹³C {¹H} NMR (126 MHz, CDCl₃): δ 164.98 (C=O), 164.30 (C=O), 155.62, 155.45, 144.73, 144.65, 143.13, 140.88, 138.55, 137.31, 131.94, 131.29, 117.51, 116.54 (aromatic C), 61.06, 60.45 (CH₂), 14.72, 14.58 (CH₃) ppm. UV-Vis [CH₂Cl₂, λ_{max} (ε × 10⁻³ M⁻¹ cm⁻¹): 339 (77.11), 371 (53.68), 525 (2.39) nm.

B. NMR Spectra

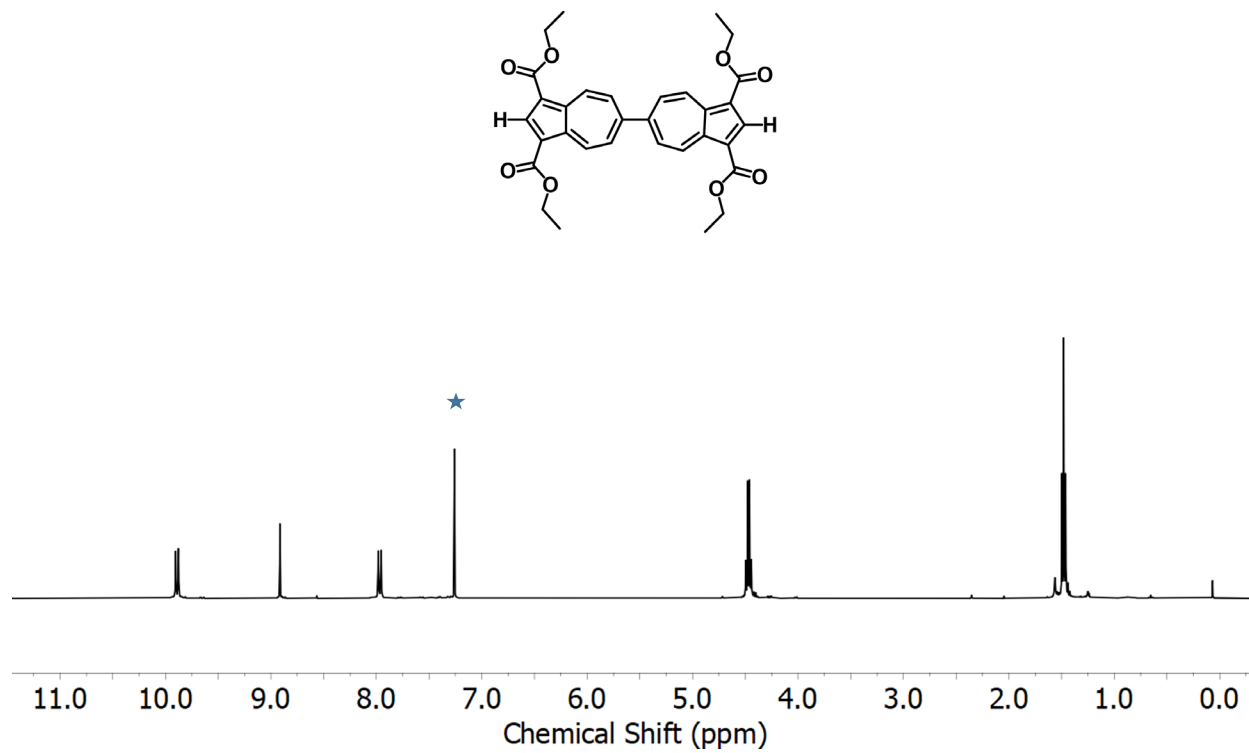


Figure S1. ¹H NMR (400 MHz, CDCl₃) spectrum of **1**; (★) denotes NMR solvent residual resonance.

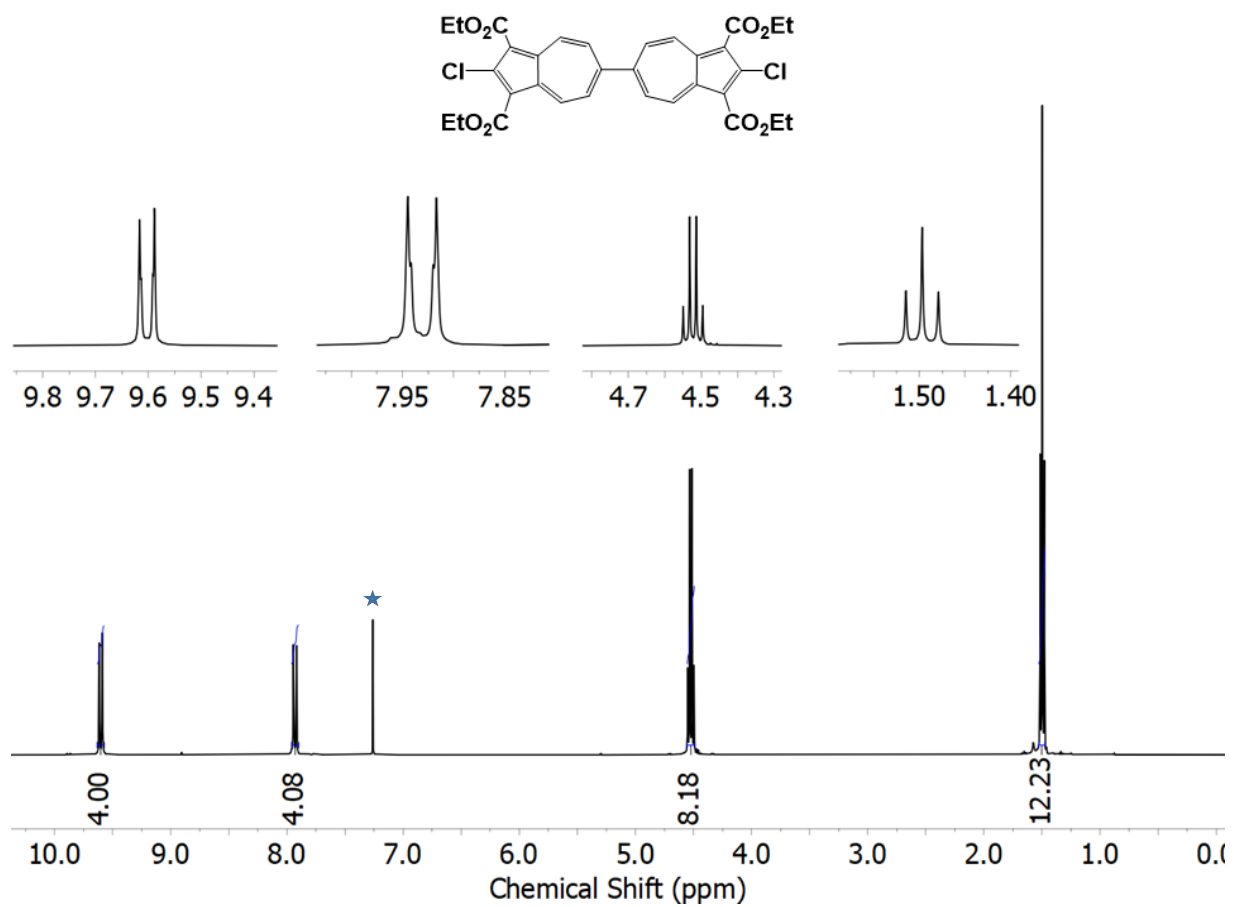


Figure S2. ^1H NMR (500 MHz, CDCl_3) spectrum of **3a**. (*) denotes NMR solvent residual resonance.

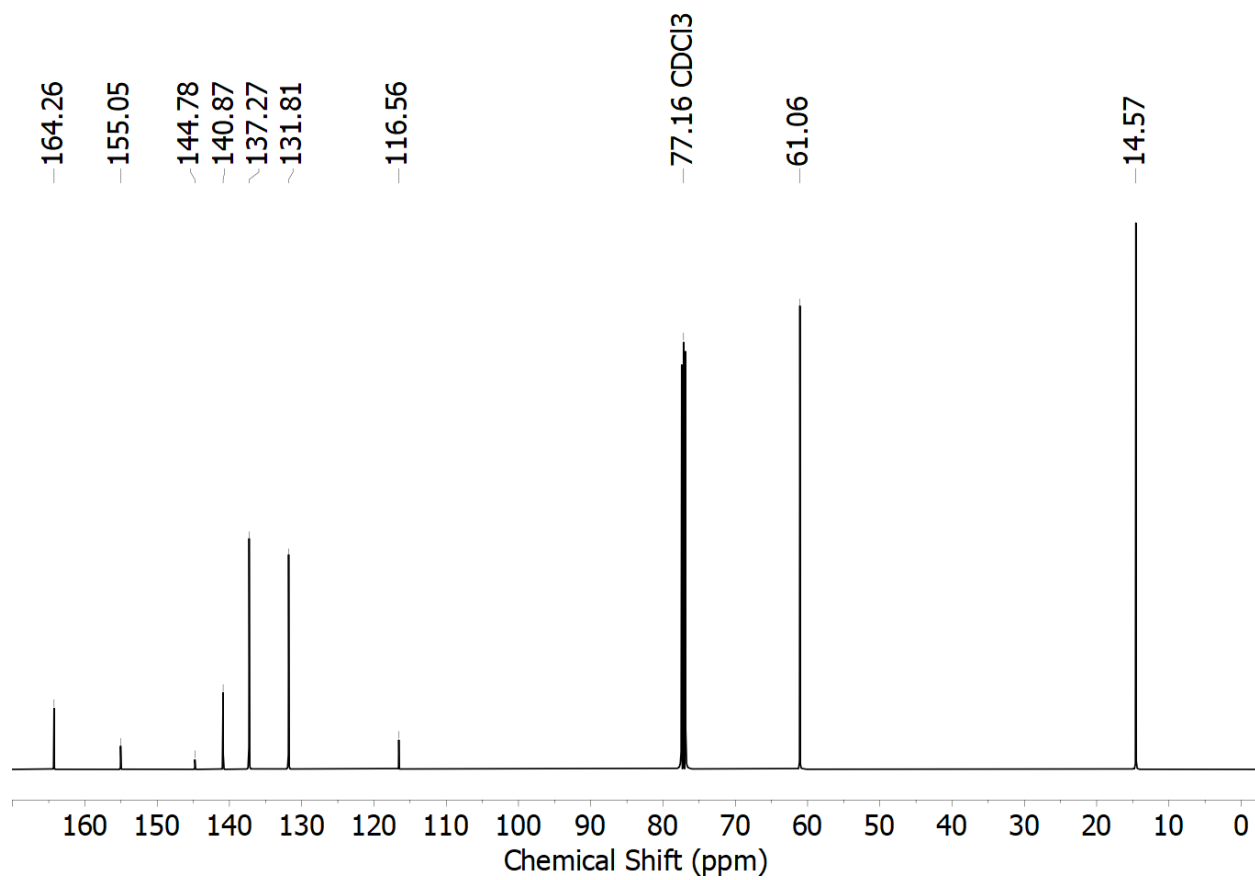


Figure S3. $^{13}\text{C}\{^1\text{H}\}$ NMR (126 MHz, CDCl_3) spectrum of **3a**.

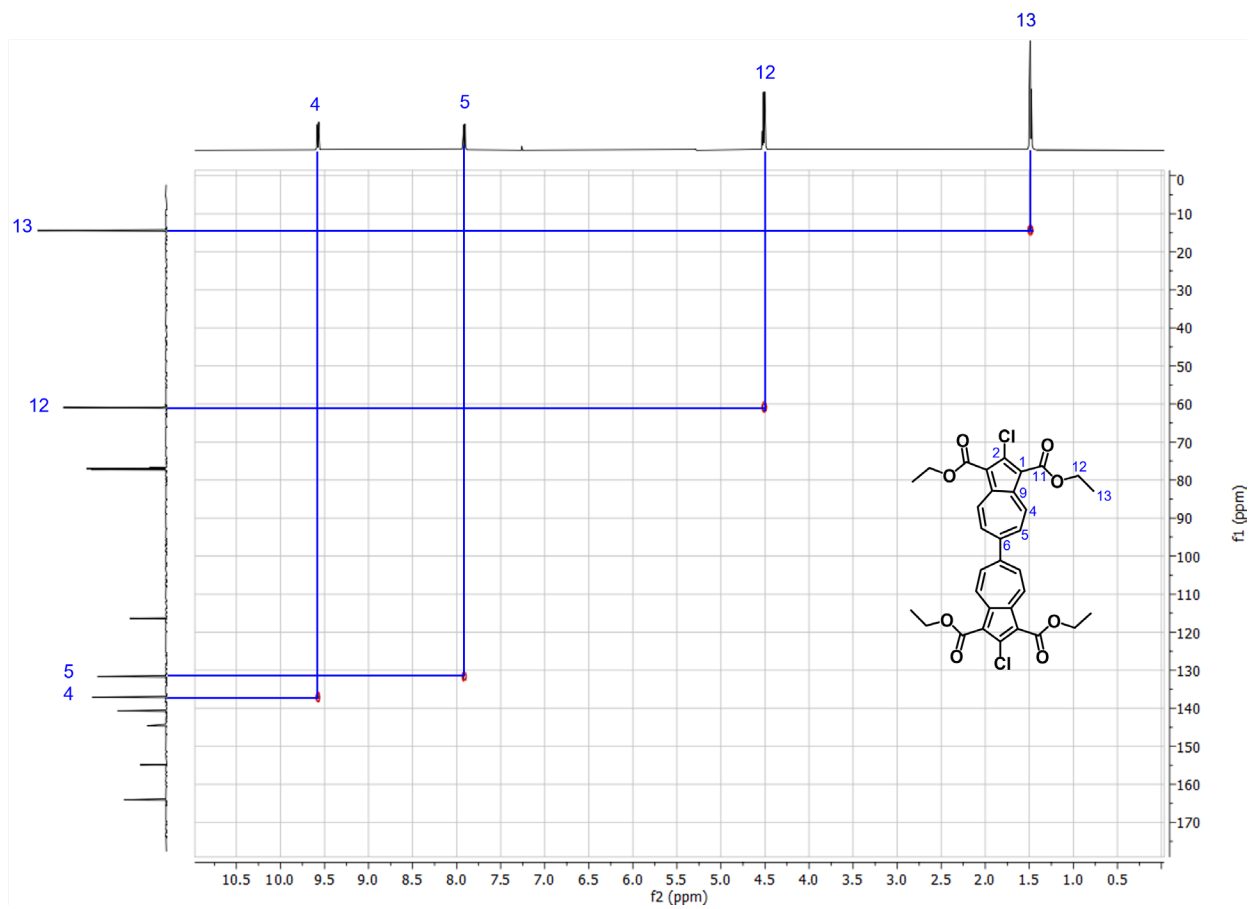


Figure S4. HSQC NMR (600 MHz, CDCl₃) spectrum of **3a**.

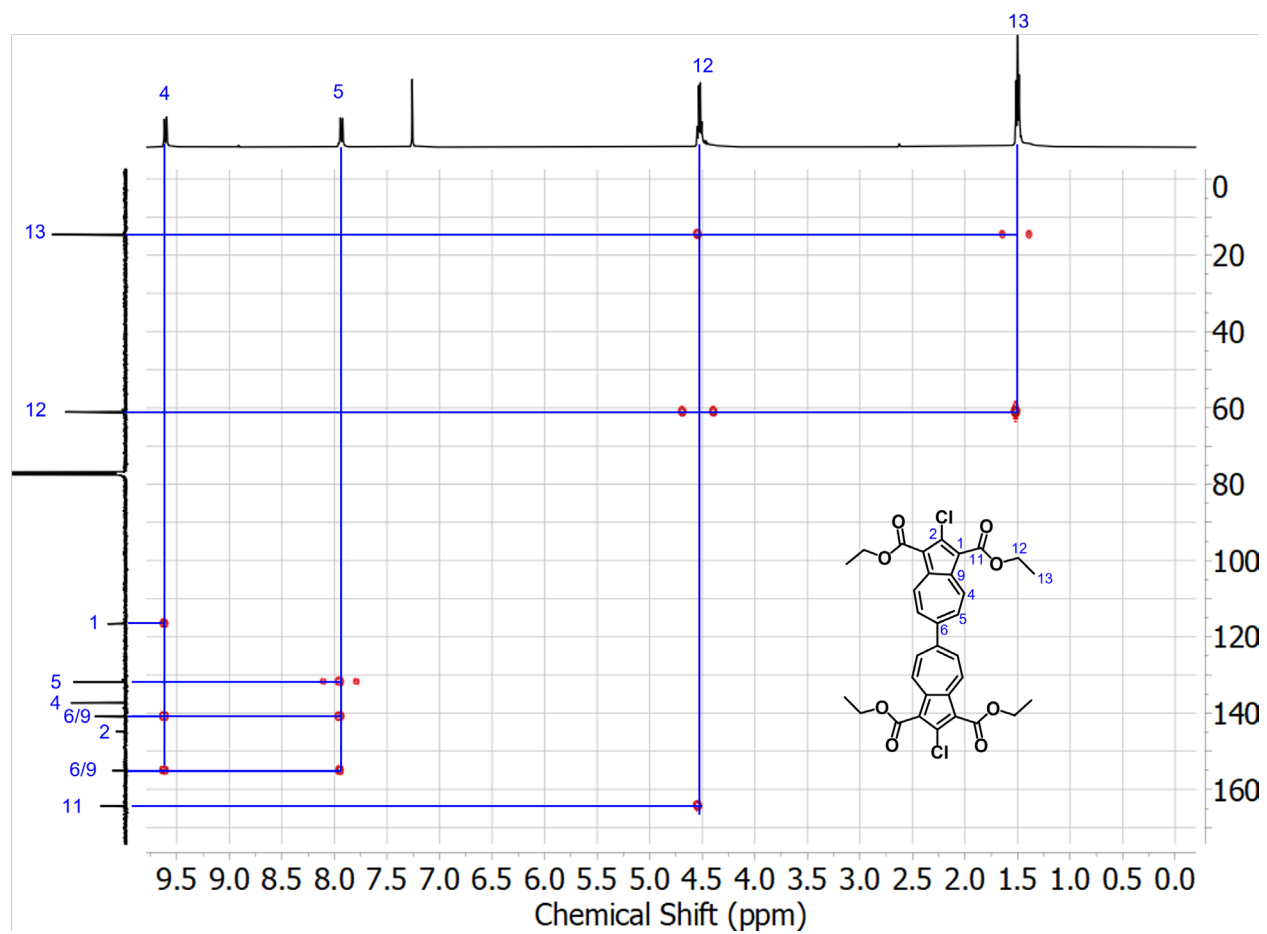


Figure S5. HMBC NMR (500 MHz, CDCl_3) spectrum of **3a**.

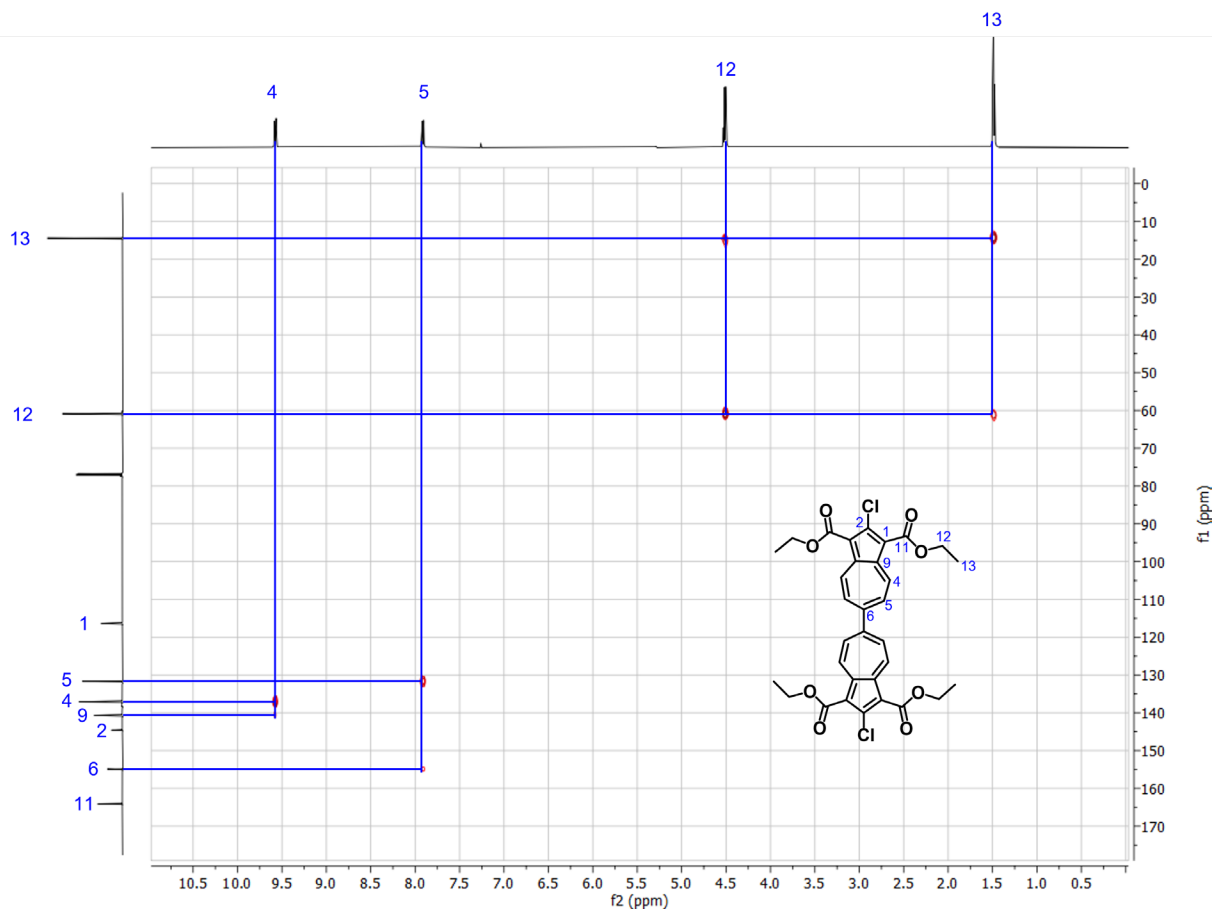


Figure S6. 1,1-ADEQUATE NMR (600 MHz, CDCl₃) spectrum of **3a**.

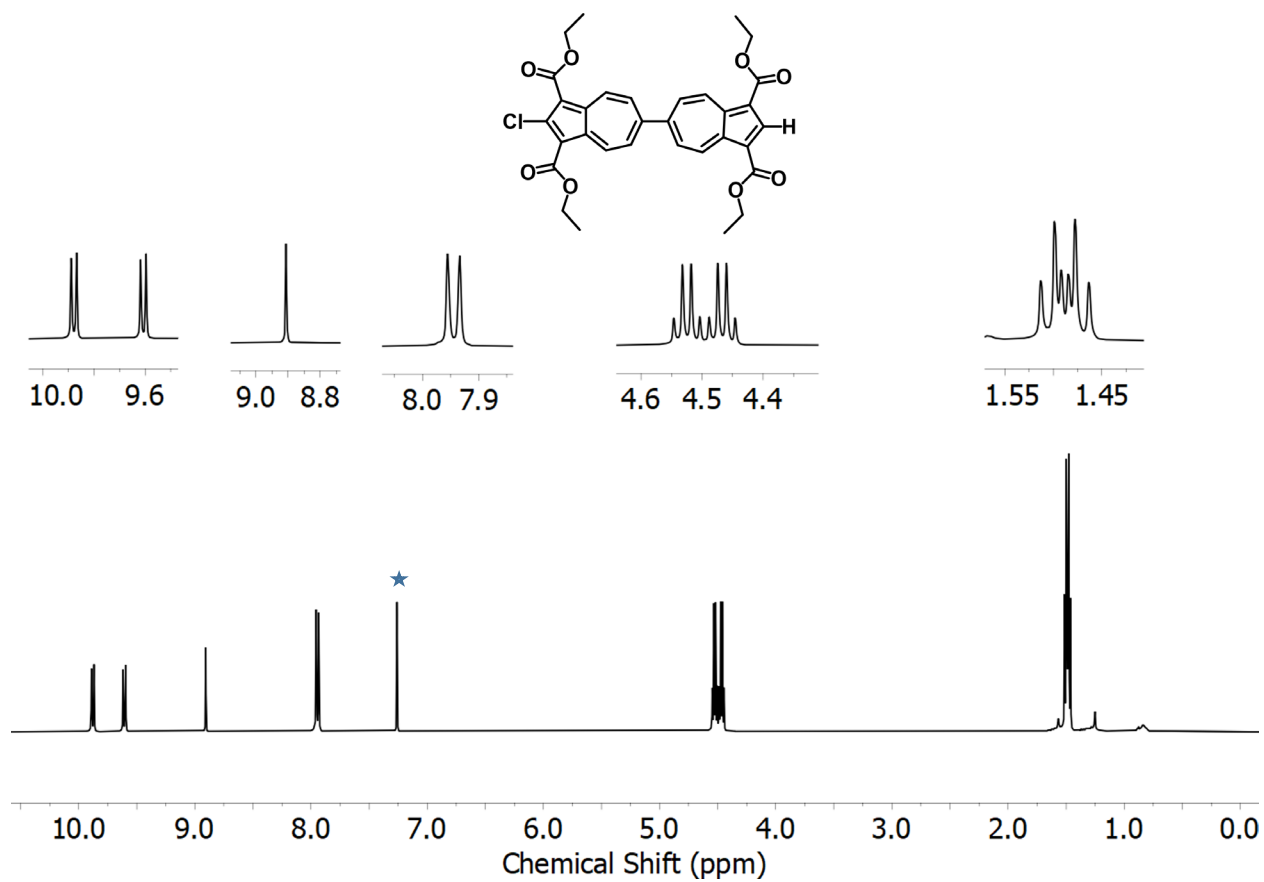


Figure S7. ¹H NMR (500 MHz, CDCl₃) spectrum of **3b**. (★) denotes NMR solvent residual resonance.

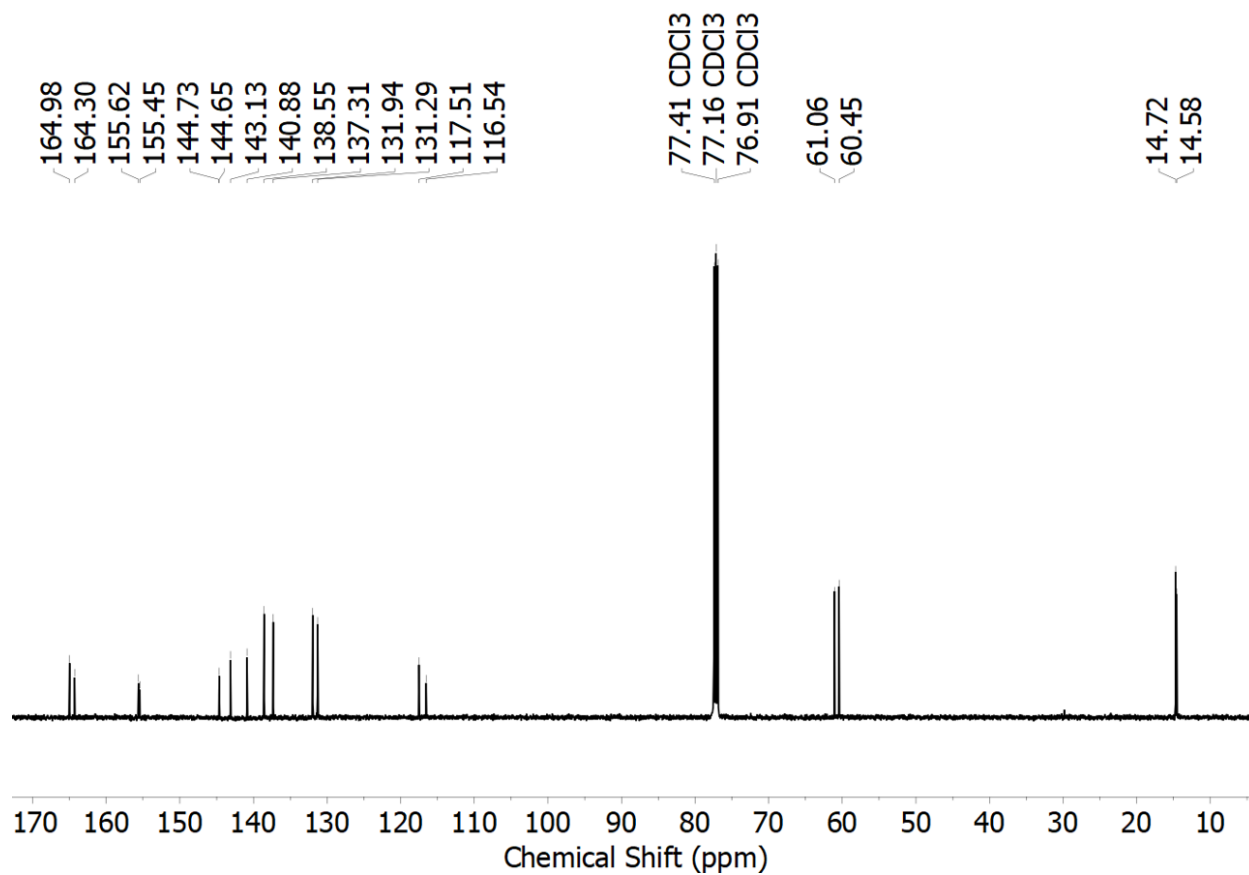


Figure S8. $^{13}\text{C}\{^1\text{H}\}$ NMR (126 MHz, CDCl_3) spectrum of **3b**.

C. Electronic absorption spectra

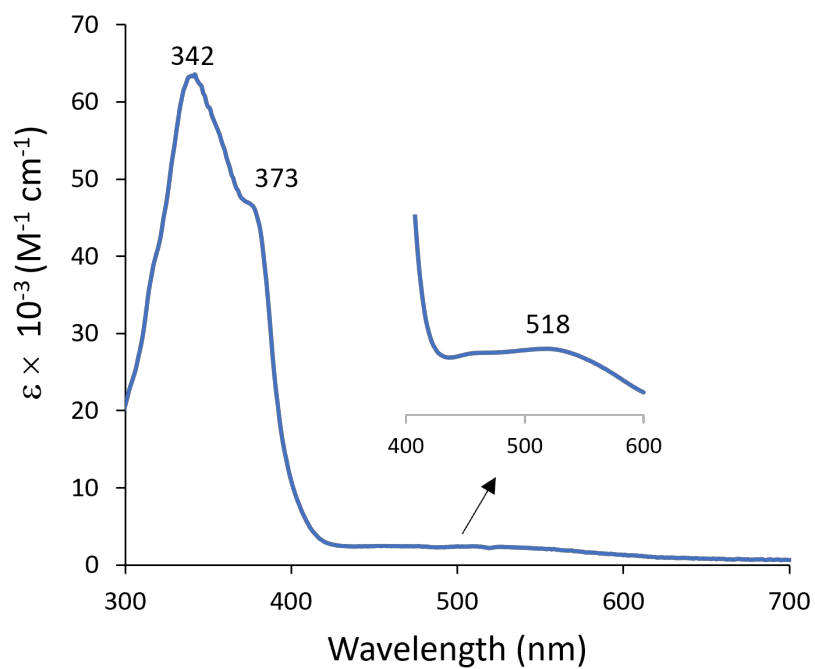


Figure S9. Electronic absorption spectrum of **1** in CH_2Cl_2 .

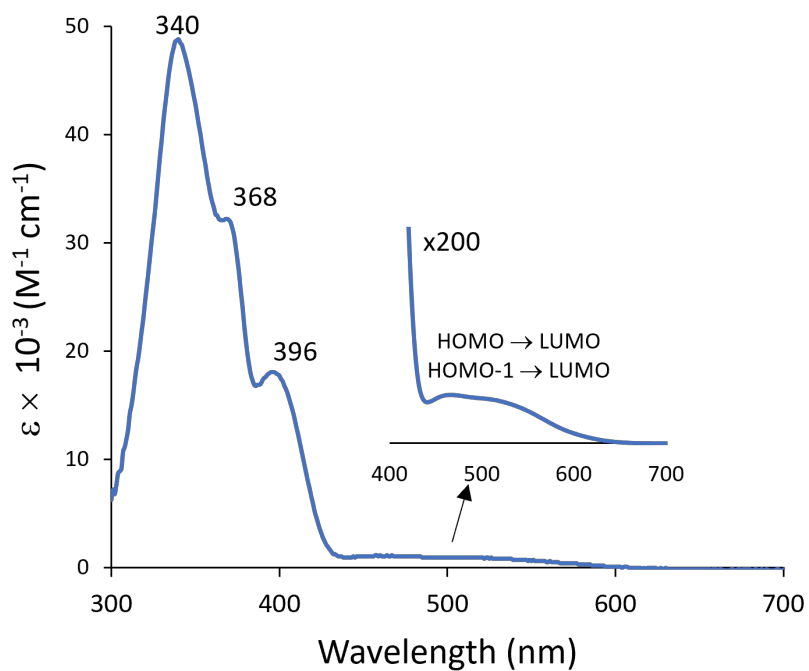


Figure S10. Electronic absorption spectrum of **3a** in CH_2Cl_2 .

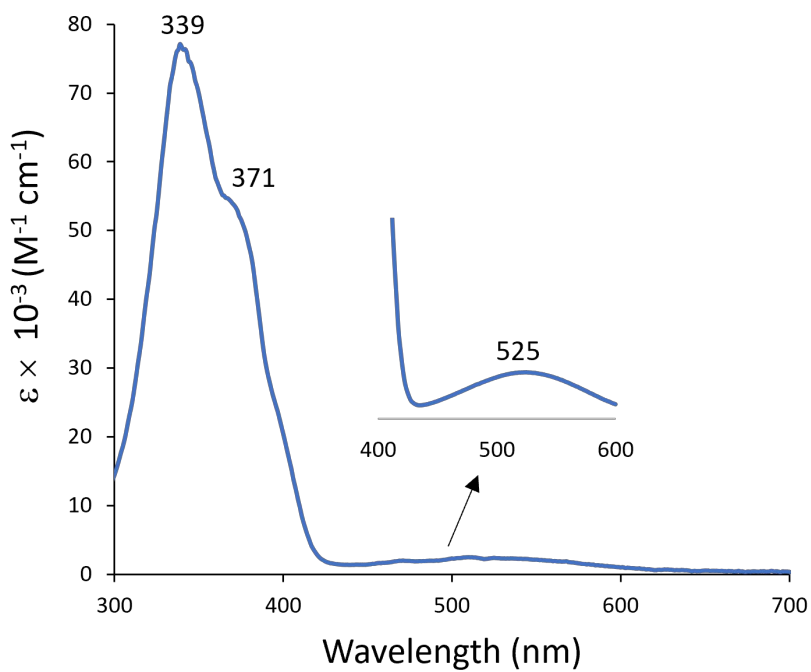


Figure S11. Electronic absorption spectrum of **3b** in CH₂Cl₂.

Table S1. Summary of the UV vis data for compounds **1**, **3a**, and **3b**.

Compound	λ_{\max} ($\epsilon \times 10^{-3} \text{ M}^{-1} \text{ cm}^{-1}$)
1	342 (63.58), 373 (47.06), 518 (2.24) nm
3a	340 (48.81), 368 (32.22), 396 (18.08), <i>ca.</i> 440-640 (1.06) nm
3b	339 (77.11), 371 (53.68), 525 (2.39) nm

D. Computational Work

D1. Calculation Details

All calculations were carried out using version 5.4 of the Q-Chem software package.¹¹ The highest-occupied and lowest-unoccupied molecular orbitals of the unfunctionalized biazulene shown in Fig. 1 were obtained from the geometry-optimized structure based on density functional theory (DFT) calculations using the B3LYP functional¹² and cc-pVDZ basis set.¹³ The time-dependent DFT (TD-DFT) calculations on **3a** also used the B3LYP functional and cc-pVDZ basis set along with the integral equation formalism polarizable continuum model¹⁴ (IEFPCM) with static dielectric constant $\epsilon = 8.93$ to represent dichloromethane as the solvent. The geometry was the B3LYP/cc-pVDZ structure with all ester groups extended away from the molecule, in contrast to the crystal structure but expected for the molecule in solution. However, this change in the molecular structure has little effect on the electronic transition energies or oscillator strengths.

To probe the minor heptafulvalene-like zwitterionic resonance forms illustrated in Figure 7, we carried out constrained DFT calculations.¹⁵ In this approach, we constrained the charge on one Cl atom to be +1 and the total charge on the carbon atoms of the 5-membered ring most distant from this Cl to be -1. These constraints should not be regarded as more than approximate models of the resonance structures. The two possible constrained electronic structures of this type (in the dichloromethane dielectric continuum model at the geometry optimized in dichloromethane) give dipole moments of 16.7 and 16.8 D; the slight difference arises from slight asymmetry in the ester substituents. Not surprisingly, these higher energy, minor resonance forms have significantly redshifted absorption features in their hypothetical electronic spectra, e.g., the weak HOMO \rightarrow LUMO transition (shifted down by 0.15 eV) occurs at 1655 nm compared to 532.5 nm for the unconstrained molecule calculation and the strongest absorption is at 624 nm corresponding to the HOMO-1 \rightarrow LUMO transition that is at 526.8 nm and weak for the unconstrained molecule.

Table S2. Cartesian coordinates of the atoms in 6,6'-biazulene used to generate its HOMO/LUMO plot in Fig. 1.

	X	Y	Z
C	5.2079964419	-1.0165006532	0.4981649608
C	3.8583619641	-0.6559040849	0.3218155463
C	3.8555447419	0.6863998447	-0.3408094919
C	5.2034315854	1.0495848952	-0.5236706134
C	6.0143197840	0.0171116858	-0.0149983706
C	2.7387889861	1.4353287302	-0.7085095298
C	1.3788672270	1.1459347156	-0.5585287697
C	0.7516307557	0.0123409923	-0.0020111625
C	1.3835420914	-1.1199755573	0.5512412723
C	2.7449071575	-1.4069065067	0.6945800963
H	5.5569098662	-1.9418497251	0.9543656122
C	-0.7539502019	0.0112587731	0.0017254191
C	-1.3828240923	1.1428008164	0.5606324244
C	-2.7431308816	1.4300842995	0.7110028810
C	-3.8588248821	0.6803698745	0.3416438983
C	-3.8596815980	-0.6605305804	-0.3238466568
C	-5.2088175508	-1.0225885947	-0.5011577235
C	-6.0166049465	0.0090216510	0.0136814064
C	-5.2072077855	1.0413970783	0.5249452759
H	-5.5564326027	-1.9475327821	-0.9591759560
C	-2.7452036587	-1.4092529153	-0.6980404763
C	-1.3842219952	-1.1207290934	-0.5539910012
H	-5.5532367781	1.9661507182	0.9845393124
H	-2.9689456248	-2.3660937761	-1.1830151653
H	-2.9656159105	2.3866352405	1.1971180558
H	-0.7083387440	-1.8782690950	-0.9577795816
H	2.9598927647	2.3931760105	-1.1927016539
H	0.7005231813	1.9038672351	-0.9574580129
H	-0.7055439721	1.9007908173	0.9612466714
H	2.9700271691	-2.3644465101	1.1775362276
H	0.7087195757	-1.8793082316	0.9534328005
H	5.5482571271	1.9758553708	-0.9813178149
H	7.1051332028	0.0178557562	-0.0177298836
H	-7.1074149248	0.0083850309	0.0159735138

Table S3. Cartesian coordinates of the atoms in **3a** used to generate Figure S12.

	X	Y	Z
C	5.2109534425	-1.0389112183	0.5529452883
C	3.8566540911	-0.6422679540	0.3192306541
C	3.8812892924	0.6597695994	-0.3586666802
C	5.2501761064	1.0463207524	-0.5128348271
C	6.0312351996	0.0008431764	0.0442351205
C	2.7699320742	1.4043937225	-0.7788104224
C	1.4067624439	1.1315531926	-0.6631399815
C	0.7449854019	0.0234198972	-0.1021315573
C	1.3653334288	-1.0937661577	0.4874372876
C	2.7179518589	-1.3800603709	0.6730372425
C	5.6848284393	2.3127804728	-1.1386015105
O	4.9321028938	3.0995236740	-1.7006969545
Cl	7.7633144191	-0.0028398287	0.1040190699
C	5.5988745725	-2.3092918647	1.2012276386
O	4.8126920198	-3.0760054380	1.7447796313
O	7.0042267207	2.5452154091	-1.0338905766
C	7.4890827245	3.7714617997	-1.6413625192
C	8.9889012373	3.8169328148	-1.4371963358
C	-0.7568892431	0.0357464988	-0.1328877459
C	-1.3948171854	1.2038639444	0.3257502452
C	-2.7522313272	1.5067173213	0.4281910362
C	-3.8766750847	0.7414592180	0.0895007653
C	-3.8806709800	-0.6150266836	-0.4739920528
C	-5.2440888953	-1.0045884527	-0.6629298304
C	-6.0410340271	0.0814978129	-0.2174621791
C	-5.2362293689	1.1510880572	0.2475489590
C	-5.6624100314	-2.3092547441	-1.2162750798
O	-4.8986667823	-3.1218259787	-1.7236291632
C	-2.7573959131	-1.4003842621	-0.7674803898
C	-1.3989262442	-1.1206030158	-0.6140187370
C	-5.6460982726	2.4548165410	0.8103858891
O	-4.9041017098	3.4226212248	0.9228525443
Cl	-7.7712329798	0.1408109821	-0.3182349885
O	-6.9245679925	2.4799389795	1.2226182899
C	-7.3990979882	3.7360155483	1.7755147264
C	-8.8393524610	3.5309315975	2.1965420967
O	-6.9803080018	-2.5463064630	-1.1014394867

C	-7.4547596047	-3.8078868124	-1.6403684313
C	-8.9524357589	-3.8592526672	-1.4222653085
O	6.9153209430	-2.5703050607	1.1361334386
C	7.3579761541	-3.8010128172	1.7664504433
C	8.8612369102	-3.8798193328	1.6010633576
H	-2.9895981075	-2.3780387849	-1.1893960528
H	-2.9823961625	2.4952220513	0.8258348805
H	-0.7369949862	-1.9242180796	-0.9453423388
H	3.0198753244	2.3397161872	-1.2788098391
H	0.7596914349	1.8958204263	-1.0997527223
H	-0.7313086957	1.9950803629	0.6825605052
H	2.9320682308	-2.3191149029	1.1828402112
H	0.6891503753	-1.8520934994	0.8890348178
H	6.8431070421	-4.6474218592	1.2854808344
H	7.0568419763	-3.7827169328	2.8254416747
H	-7.2988184985	4.5188892990	1.0073255216
H	-6.7547928097	4.0126656814	2.6244053081
H	6.9799083556	4.6245183966	-1.1660428015
H	7.2148401278	3.7688681102	-2.7077944563
H	-6.9321660800	-4.6293985445	-1.1258636671
H	-7.1886673839	-3.8572162517	-2.7078656811
H	-9.4676982585	3.2503702360	1.3368502552
H	-9.2337519115	4.4664904804	2.6232773113
H	-8.9184342694	2.7415980531	2.9605980620
H	9.3572937560	-3.0226087111	2.0826634659
H	9.1419887404	-3.8933966540	0.5361938825
H	9.2345659744	-4.8042592957	2.0689389636
H	9.4791734041	2.9539379884	-1.9143729943
H	9.2431756416	3.8152731376	-0.3655698703
H	9.3931025227	4.7374955101	-1.8867910883
H	-9.1983535499	-3.8050880793	-0.3500118345
H	-9.3495977451	-4.8061307213	-1.8205727307
H	-9.4559132494	-3.0271359413	-1.9389027895

Table S4. Allowed transition wavelengths, oscillator strengths, and transition orbital amplitudes obtained from the TD-DFT/B3LYP/cc-pVDZ calculations. (Transition wavelengths correspond to the transition energies shifted down by 0.15 eV as shown in Figure S12).

Adjusted Transition Wavelength (nm)	Oscillator Strength	Transition Orbital Amplitudes
532.5	0.0106	0.9529 HOMO → LUMO
526.8	0.0033	0.9530 HOMO-1 → LUMO
404.0	0.8249	0.9481 HOMO-2 → LUMO 0.2334 HOMO → LUMO+1
379.8	0.00075	-0.2287 HOMO-1 → LUMO 0.9409 HOMO → LUMO+2
377.0	0.0018	0.9388 HOMO-1 → LUMO+2 -0.2232 HOMO → LUMO
368.5	0.00014	0.8040 HOMO-3 → LUMO 0.4965 HOMO-1 → LUMO+1 -0.2740 HOMO → LUMO+3
358.4	0.1393	-0.2264 HOMO-1 → LUMO+1 0.3879 HOMO-1 → LUMO+3 0.7795 HOMO → LUMO+1 -0.3958 HOMO → LUMO+3
355.9	0.0570	0.6254 HOMO-1 → LUMO+1 0.4089 HOMO-1 → LUMO+3 0.2810 HOMO → LUMO+1 0.5733 HOMO → LUMO+3
341.0	0.00006	0.3434 HOMO-4 → LUMO -0.2669 HOMO-3 → LUMO 0.6959 HOMO-2 → LUMO+2 0.3017 HOMO-1 → LUMO+1 -0.4369 HOMO → LUMO+3
337.2	1.4634	0.2696 HOMO-5 → LUMO -0.3002 HOMO-3 → LUMO+2 0.7200 HOMO-1 → LUMO+3 -0.4114 HOMO → LUMO+1
336.7	0.0214	0.9061 HOMO-4 → LUMO -0.2749 HOMO-2 → LUMO+2
335.7	0.1465	0.9061 HOMO-5 → LUMO -0.2310 HOMO-1 → LUMO+3
329.0	0.0066	0.9666 HOMO-6 → LUMO
324.7	0.0055	0.9622 HOMO-7 → LUMO
322.2	0.0569	0.2125 HOMO-14 → LUMO 0.8810 HOMO-2 → LUMO+1

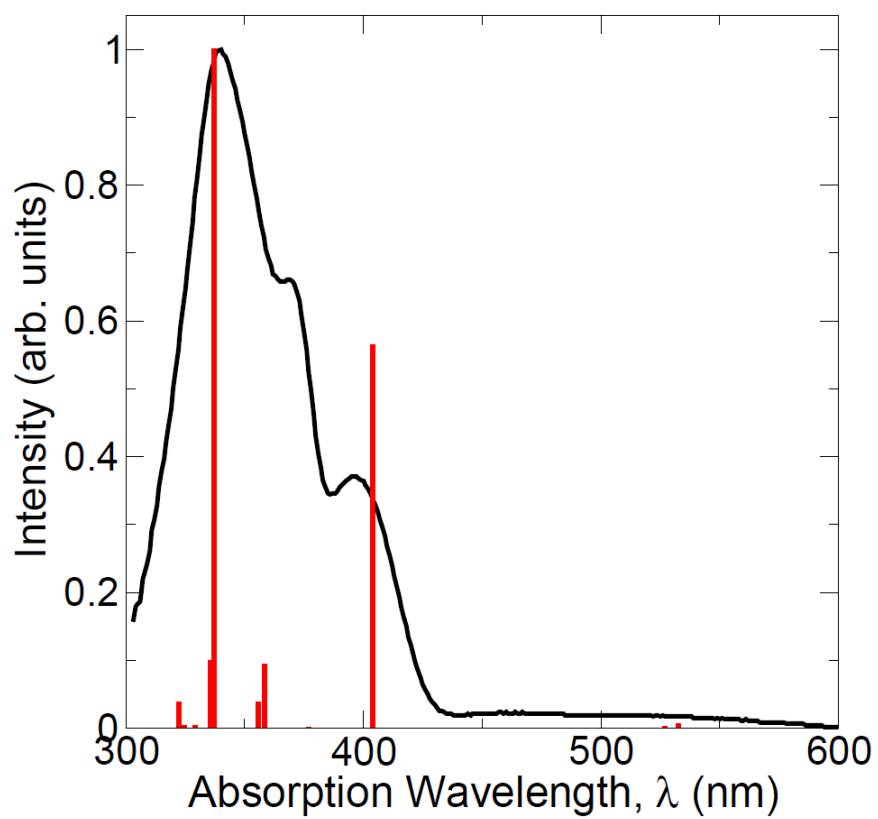


Figure S12. Experimental vs. simulated electronic spectra of **3a**. The simulated transition wavelengths are shifted down by a 0.15 eV increment.

E. Electrochemistry

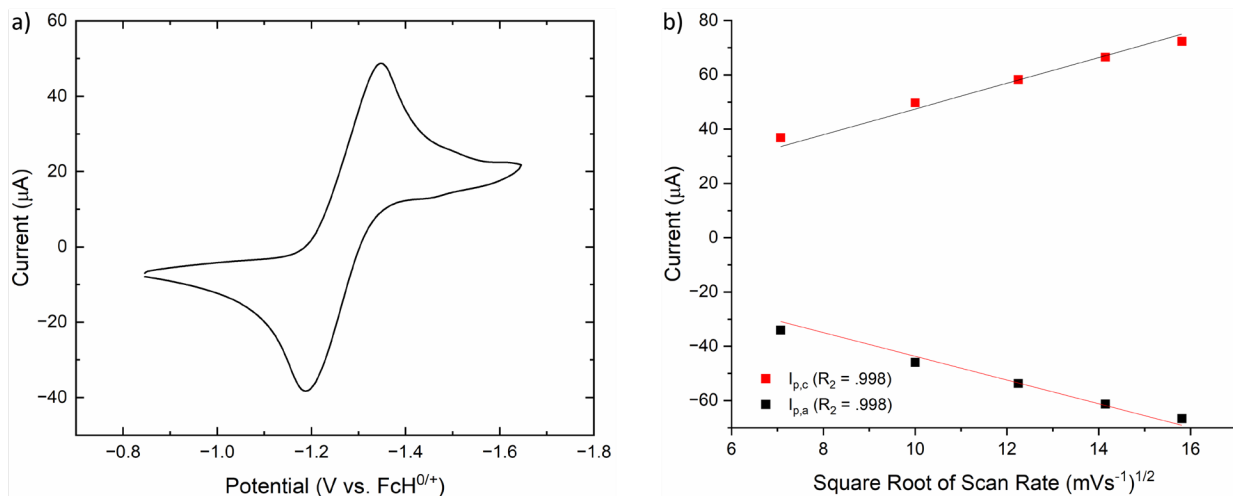


Figure S13. a) Cyclic voltammogram of 1.1 mM solution of **1** in 0.1 M $[\text{nBu}_4\text{N}]^+[\text{PF}_6]^-/\text{CH}_2\text{Cl}_2$ vs. external $\text{Cp}_2\text{Fe}^{0/+}$ at 22 °C (scan rate = 100 mV/s). b) Scan rate dependence of **1** in 0.1 M $[\text{nBu}_4\text{N}]^+[\text{PF}_6]^-/\text{CH}_2\text{Cl}_2$.

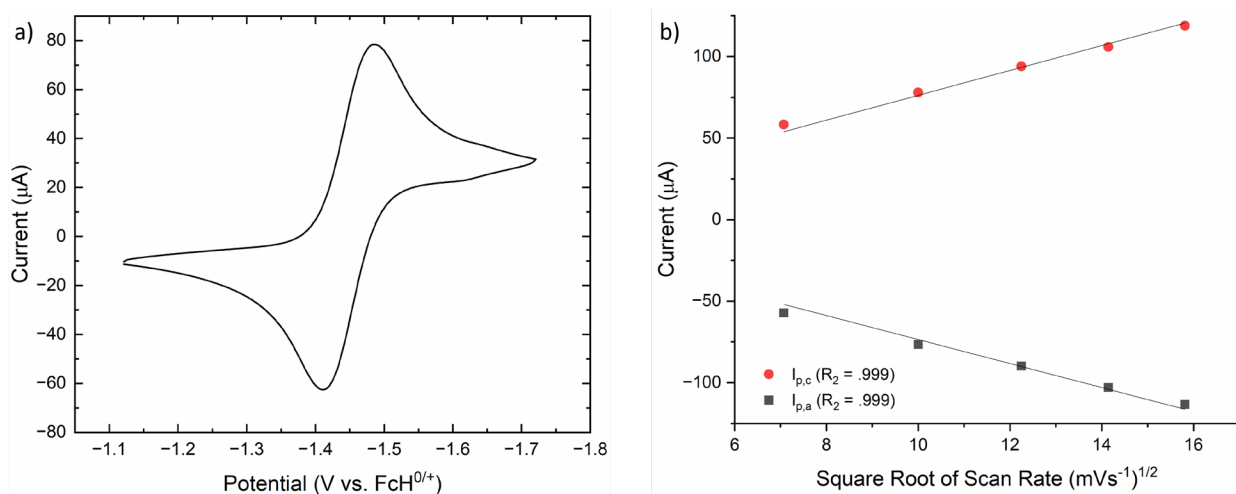


Figure S14. a) Cyclic voltammogram of 2.2 mM solution of **2b** in 0.1 M $[\text{nBu}_4\text{N}]^+[\text{PF}_6]^-/\text{CH}_2\text{Cl}_2$ vs. external $\text{Cp}_2\text{Fe}^{0/+}$ at 22 °C (scan rate = 100 mV/s). b) Scan rate dependence of **2b** in 0.1 M $[\text{nBu}_4\text{N}]^+[\text{PF}_6]^-/\text{CH}_2\text{Cl}_2$.

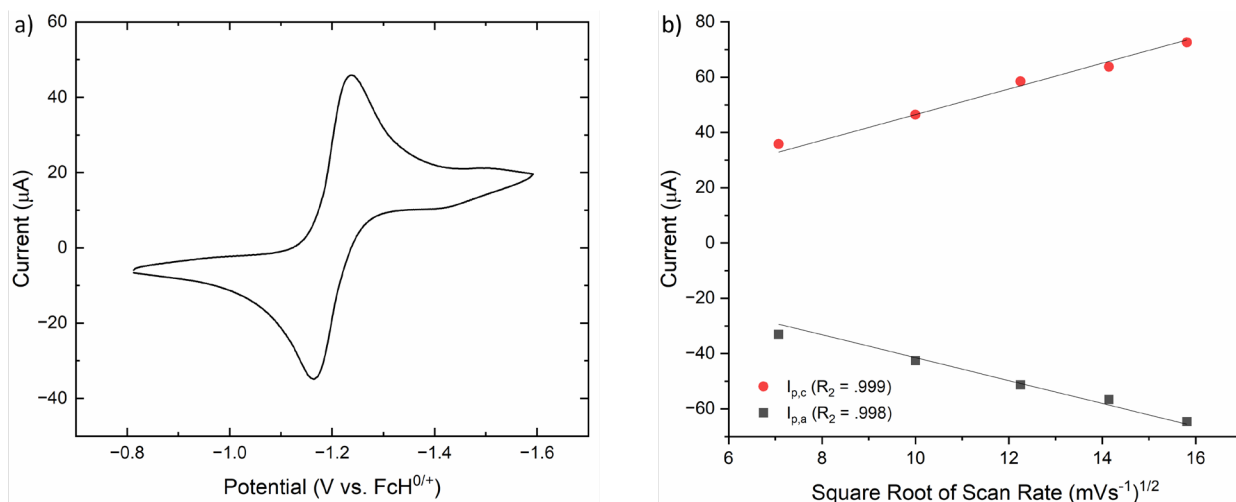


Figure S15. a) Cyclic voltammogram of 1.6 mM solution of **3a** in 0.1 M [ⁿBu₄N]⁺[PF₆]⁻/CH₂Cl₂ vs. external Cp₂Fe^{0/+} at 22 °C (scan rate = 100 mV/s). b) Scan rate dependence of **3a** in 0.1 M [ⁿBu₄N]⁺[PF₆]⁻/CH₂Cl₂.

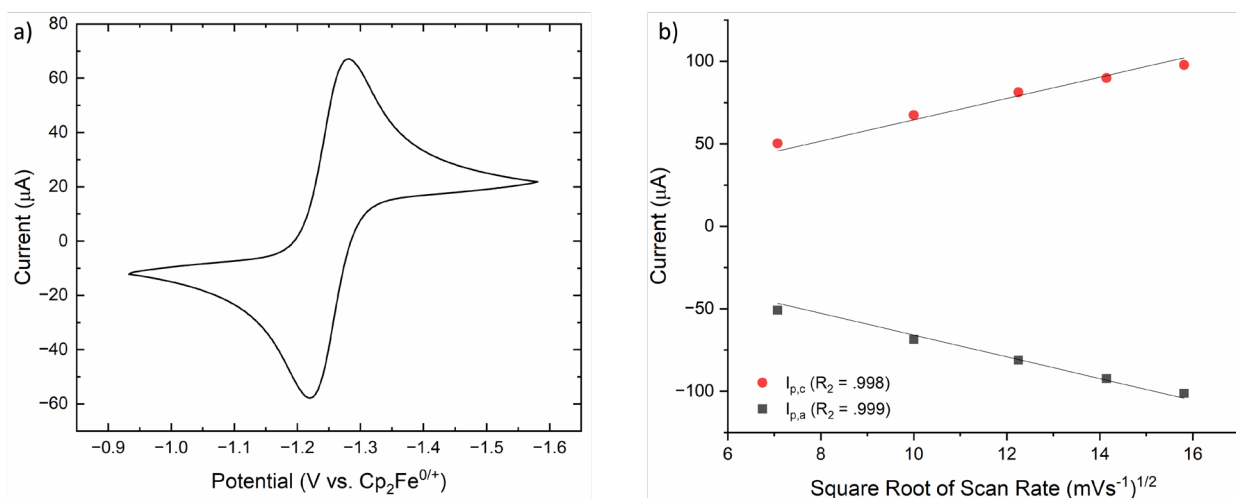


Figure S16. a) Cyclic voltammogram of 2.0 mM solution of **3b** in 0.1 M [ⁿBu₄N]⁺[PF₆]⁻/CH₂Cl₂ vs. external Cp₂Fe^{0/+} at 22 °C (scan rate = 100 mV/s). b) Scan rate dependence of **3b** in 0.1 M [ⁿBu₄N]⁺[PF₆]⁻/CH₂Cl₂.

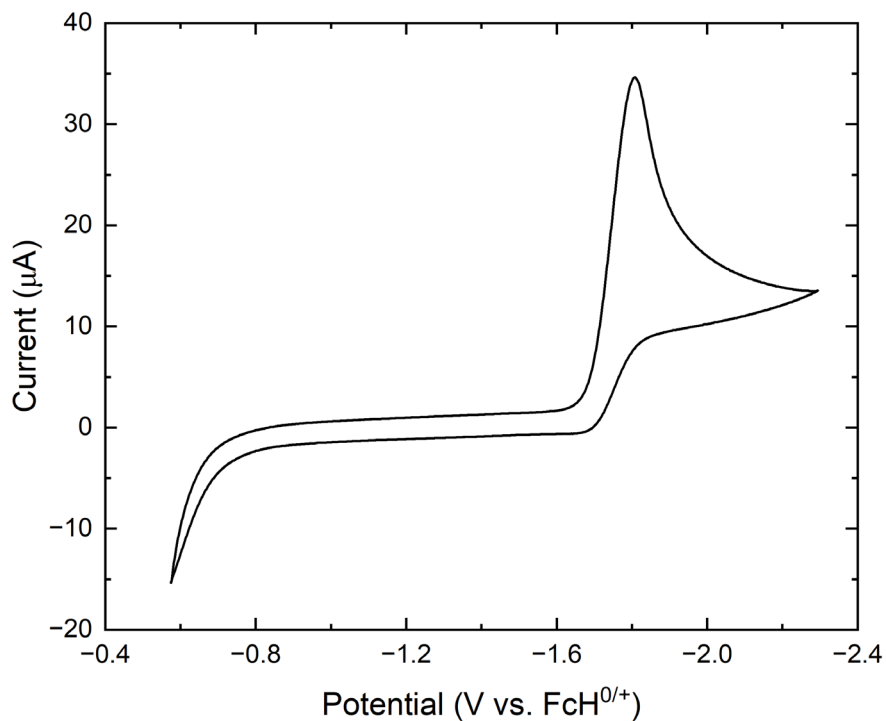


Figure S17. Cyclic voltammogram of 2.0 mM solution of 1,3-diethoxycarbonylazulene in 0.1 M [ⁿBu₄N]⁺[PF₆]⁻/CH₂Cl₂ vs. external Cp₂Fe^{0/+} at 22 °C (scan rate = 100 mV/s).

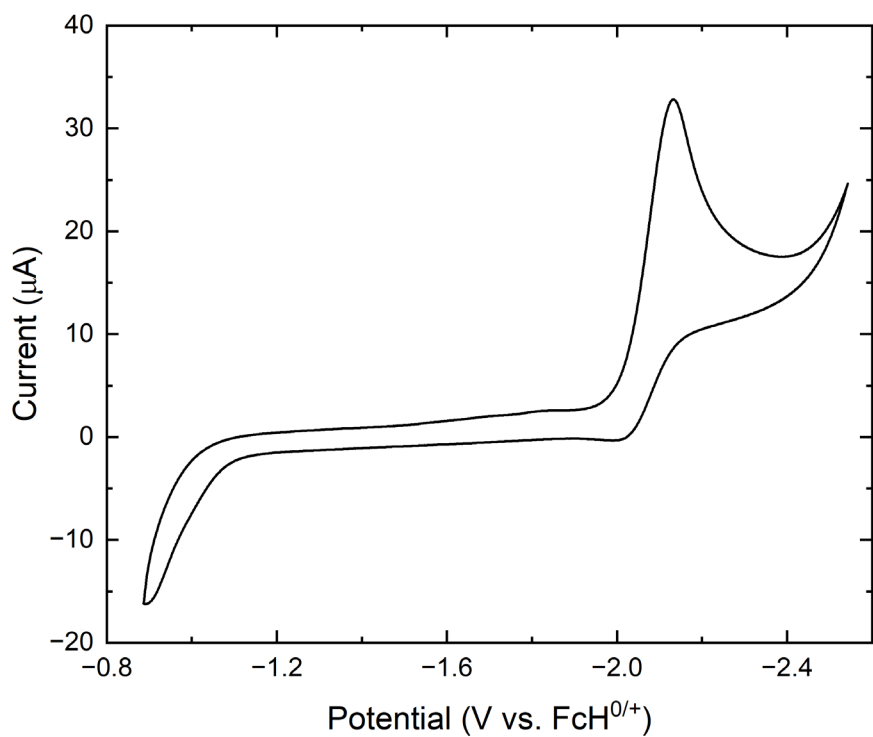


Figure S18. Cyclic voltammogram of 2.0 mM solution of 2-amino-1,3-diethoxycarbonylazulene in 0.1 M [ⁿBu₄N]⁺[PF₆]⁻/CH₂Cl₂ vs. external Cp₂Fe^{0/+} at 22 °C (scan rate = 100 mV/s).

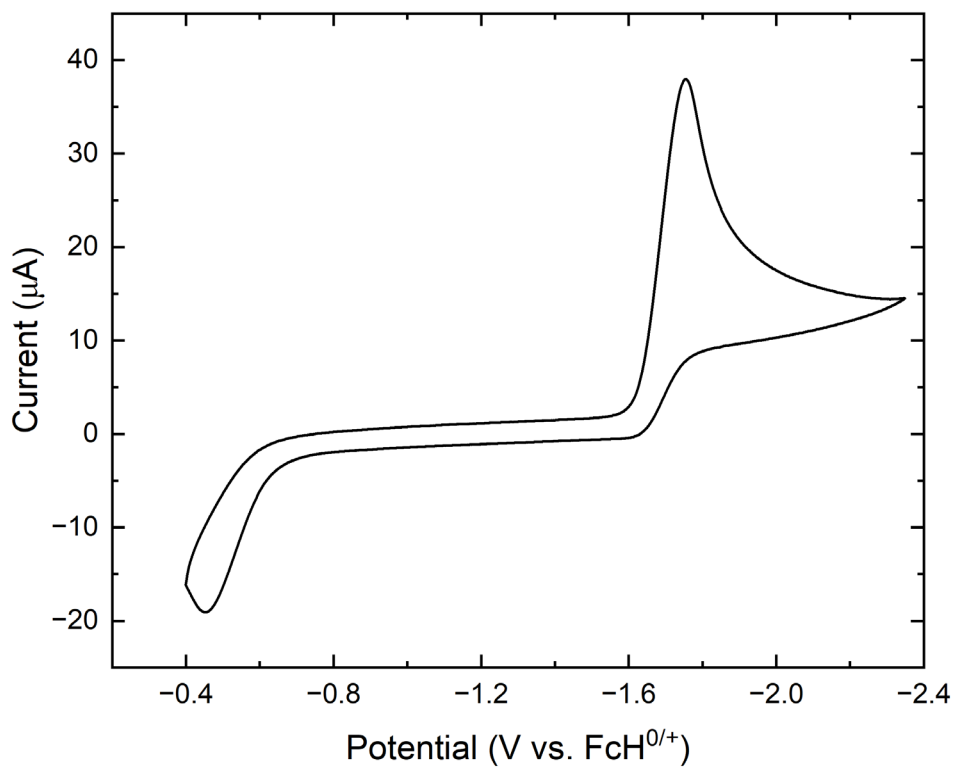


Figure S19. Cyclic voltammogram of 2.0 mM solution of 2-chloro-1,3-diethoxycarbonylazulene in 0.1 M $[\text{mBu}_4\text{N}]^+[\text{PF}_6]^-/\text{CH}_2\text{Cl}_2$ vs. external $\text{Cp}_2\text{Fe}^{0/+}$ at 22 °C (scan rate = 100 mV/s).

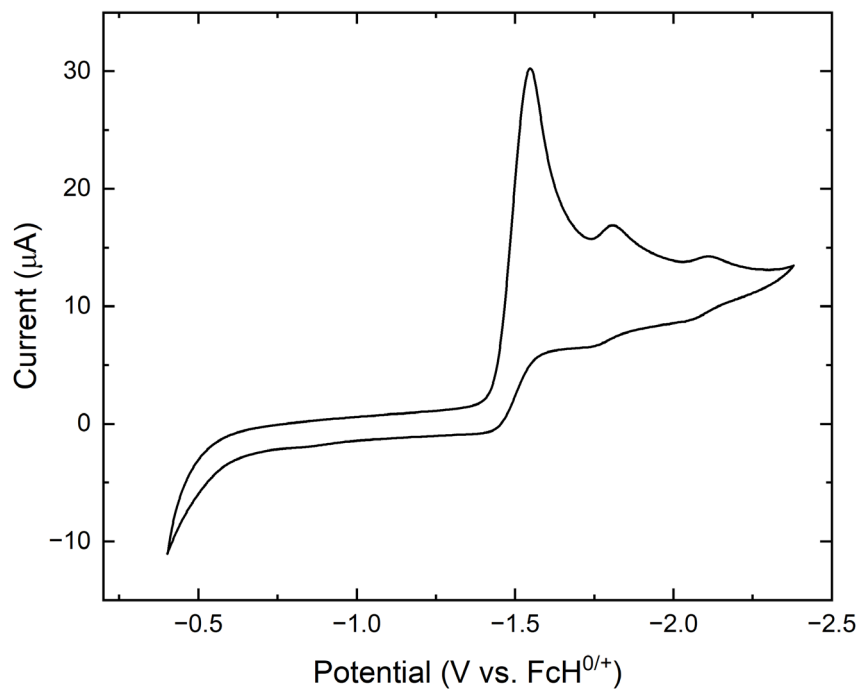
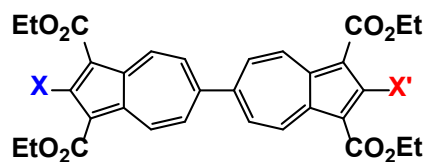


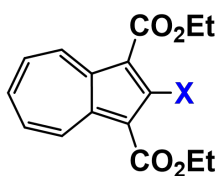
Figure 20. Cyclic voltammogram of 2.0 mM solution of 2-isocyano-1,3-diethoxycarbonylazulene in 0.1 M $[\text{mBu}_4\text{N}]^+[\text{PF}_6]^-/\text{CH}_2\text{Cl}_2$ vs. external $\text{Cp}_2\text{Fe}^{0/+}$ at 22 °C (scan rate = 100 mV/s).

Table S5. $E_{1/2}$ potentials and σ_p parameters for Fig. 4.



Ref.	X	X'	$\sigma_p(X) + \sigma_p(X')$	$E_{1/2}$ (V) $Az^0 \rightarrow Az^{2-}$	$\Delta E_{p,c-p,a}$ (mV)	$i_{p,c}/i_{p,a}$
1	-NH ₂	-NH ₂	-0.66 + -0.66 = -1.32	-1.64	118	1.07
This work	-NH ₂	-H	-0.66 + 0.00 = -0.66	-1.45	76	1.02
This work	-H	-H	0.00 + 0.00 = 0.00	-1.27	159	1.08
This work	-Cl	-H	0.23 + 0.00 = 0.23	-1.25	63	0.98
This work	-Cl	-Cl	0.23 + 0.23 = 0.46	-1.20	72	1.09
2	-NC	-H	0.49 + 0.00 = 0.49	-1.16	170	0.98
1	-NC	-NC	0.49 + 0.49 = 0.98	-1.02	60	1.0

Table S6. $E_{p,c}$ potentials and σ_p parameters for Fig. 5.



X	$\sigma_p(X)$	$E_{p,c}$ (V) $Az^0 \rightarrow Az^{2-}$
-NH ₂	-0.66	-2.16
-H	0.00	-1.84
-Cl	0.23	-1.79
-NC	0.49	-1.58

F. X-Ray Crystallography

F1. Experimental and Refinement Model Description

Table S6 contains crystal data, collection parameters, and refinement criteria for the crystal structure of **3a**. A dark red crystal coated with STP oil was placed on the tip of a Mitigen micromount (MiTeGen, LLC, Ithaca, NY) and X-ray intensity data were measured at low temperature (173(2) K, Oxford Cryosystems desktop cooler, Oxford Cryosystems Ltd., Oxford) with graphite monochromated Mo K α radiation ($\lambda = 0.71073 \text{ \AA}$) on a Rigaku XtaLAB mini diffractometer.¹⁶ The intensity data were corrected for absorption and decay (ChrysAlis PRO). Final cell constants were calculated based on the xyz centroids of 5126 strong reflections from the actual data collection after integration (ChrysAlis PRO). Utilizing Olex2¹⁷, the structure was solved with SHELXT 2018/2¹⁸ and refined with SHELXL 2018/3¹⁹. A direct-methods solution identified most of the non-hydrogen atoms from the E-map. Full-matrix least-squares/difference Fourier cycles were performed that located the remaining nonhydrogen atoms. All non-hydrogen atoms were refined with anisotropic displacement parameters. All of the hydrogen atoms were placed in calculated positions and refined in the riding-model approximation with C-H distances = 0.99, 0.98, and 0.95 \AA for the methylene C-H, methyl C-H, and aromatic C-H, respectively, along with $U_{\text{iso}}(\text{H}) = k U_{\text{eq}}(\text{C})$, $k = 1.2$ for all C-H except methyl groups where $k = 1.5$. CCDC entry 2300779 contains the relevant crystallographic data associated with this article. These data can be accessed free of charge from the Cambridge Crystallographic Data Centre.

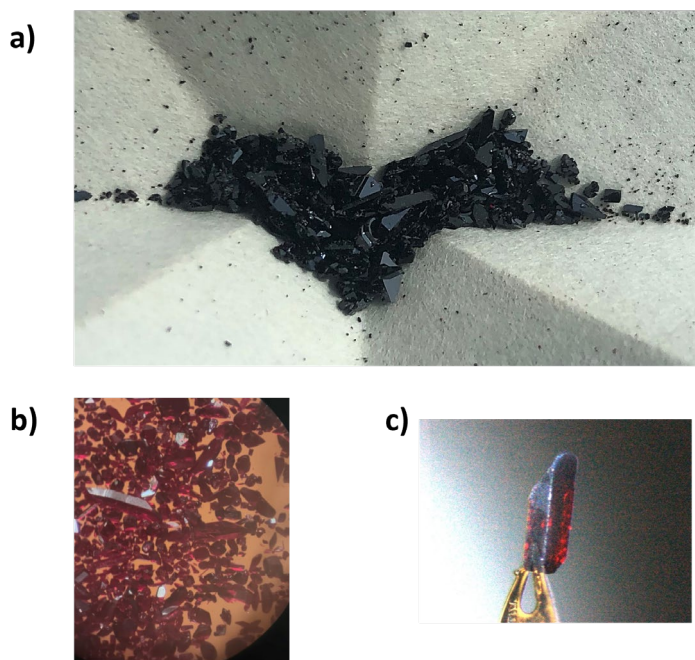


Figure S21. a) Bulk crystalline sample of **3a**; b) crystals of **3a** under microscopic amplification; c) crystal of **3a** selected for X-ray diffraction study.

Table S7. Crystal data and structure refinement for **3a**.

Empirical formula	C ₃₂ H ₂₈ Cl ₂ O ₈
Formula weight	611.44
Temperature/K	173.15
Crystal system	triclinic
Space group	P-1 (no. 2)
a/Å	9.9510(8)
b/Å	10.5842(9)
c/Å	14.9945(12)
α/°	96.395(7)
β/°	99.389(7)
γ/°	117.914(8)
Volume/Å ³	1344.5(2)
Z	2
ρ _{calc} /cm ³	1.51
μ/mm ⁻¹	0.298
F(000)	636
Crystal size/mm ³	0.45 × 0.18 × 0.1
Radiation	Mo Kα (λ = 0.71073)
2θ range for data collection/°	4.46 to 61.016
Index ranges	-14 ≤ h ≤ 14, -15 ≤ k ≤ 15, -21 ≤ l ≤ 21
Reflections collected	18156
Independent reflections	8070 [R _{int} = 0.0331, R _{sigma} = 0.0471]
Data/restraints/parameters	8070/0/383
Goodness-of-fit on F ²	1.062
Final R indexes [I > 2σ(I)]	R ₁ = 0.0527, wR ₂ = 0.1357
Final R indexes [all data]	R ₁ = 0.0753, wR ₂ = 0.1598
Largest diff. peak/hole / e Å ⁻³	0.49/-0.59

Table S8. Fractional Atomic Coordinates ($\times 10^4$) and Equivalent Isotropic Displacement Parameters ($\text{\AA}^2 \times 10^3$) for **3a**. U_{eq} is defined as 1/3 of the trace of the orthogonalised U_{ij} tensor.

Atom	<i>x</i>	<i>y</i>	<i>z</i>	<i>U</i> (eq)
Cl1	14147.7(5)	5032.9(5)	10952.0(3)	31.69(13)
Cl2	-256.7(7)	1553.8(6)	3658.4(4)	45.64(16)
O6	22.4(16)	-983.3(15)	3553.0(10)	34.8(3)
O4	11632.4(16)	2324.2(16)	11060.8(10)	35.5(3)
O2	14758.0(16)	7761.7(15)	10383.4(9)	35.2(3)
O1	14189.8(17)	7421.7(17)	8855.8(10)	38.7(4)
O8	2926.4(18)	5698.8(16)	5705.0(10)	36.4(3)
O7	1193.4(18)	4655.7(17)	4362.5(10)	36.8(3)
O3	9194.6(18)	1439(2)	10339.0(14)	60.2(6)
O5	2094(2)	-1051(2)	4219.5(14)	63.0(6)
C3	11072(2)	3543.4(19)	10007.6(12)	23.3(3)
C10	10120(2)	3703.2(19)	9283.1(11)	22.2(3)
C9'	3655(2)	3383(2)	5532.5(12)	24.0(3)
C9	11093(2)	5016.3(19)	8995.6(11)	22.5(3)
C1'	2403(2)	3420(2)	4980.7(12)	25.5(4)
C10'	3414(2)	1928(2)	5272.5(12)	25.4(3)
C4	8553(2)	2774(2)	8914.9(12)	25.6(3)
C1	12592(2)	5637.4(19)	9570.4(12)	23.5(3)
C20	2096(2)	4623(2)	4967.1(12)	26.9(4)
C6	7833(2)	3816(2)	7631.1(12)	24.4(3)
C2	12565(2)	4734.1(19)	10170.7(11)	22.5(3)
C8	10653(2)	5578(2)	8295.3(12)	25.2(3)
C11	13916(2)	7010(2)	9541.7(13)	26.6(4)
C6'	6468(2)	3468(2)	6883.0(12)	25.8(4)
C14	10524(2)	2340(2)	10467.3(13)	28.8(4)
C5	7563(2)	2829(2)	8194.0(13)	27.8(4)
C8'	4906(2)	4528(2)	6182.0(12)	26.8(4)
C7'	6130(2)	4569(2)	6772.4(13)	27.9(4)
C7	9225(2)	5054(2)	7694.2(12)	26.8(4)
C2'	1436(2)	2036(2)	4415.0(12)	26.6(4)
C3'	2027(2)	1109(2)	4568.9(12)	27.3(4)
C4'	4332(2)	1393(2)	5656.1(13)	29.8(4)
C17	1410(2)	-393(2)	4117.4(13)	31.7(4)
C5'	5648(2)	2064(2)	6366.1(13)	30.8(4)
C18	-632(2)	-2462(2)	3073.5(14)	35.1(4)
C12	16192(2)	9076(2)	10476.7(15)	37.7(5)
C21	2634(3)	6901(2)	5737.9(16)	37.8(5)

C15	11162(3)	1115(2)	11500.7(16)	40.3(5)
C13	16648(3)	9880(2)	11443.8(16)	41.7(5)
C19	-2086(3)	-2842(3)	2394.4(16)	44.8(6)
C22	3811(3)	8054(3)	6531.4(16)	44.8(5)
C16	12575(3)	1258(3)	12088.9(18)	45.4(5)

Table S9. Anisotropic Displacement Parameters ($\text{\AA}^2 \times 10^3$) for **3a**. The anisotropic displacement factor exponent takes the form: $-2\pi^2[h^2a^*2U_{11}+2hka^*b^*U_{12}+\dots]$.

Atom	U_{11}	U_{22}	U_{33}	U_{23}	U_{13}	U_{12}
C11	22.0(2)	38.0(3)	29.4(2)	9.20(18)	-1.12(17)	12.33(19)
C12	38.0(3)	44.6(3)	46.9(3)	-9.9(2)	-16.0(2)	27.1(2)
O6	29.0(7)	30.9(7)	36.3(7)	-7.3(6)	-5.0(6)	15.5(6)
O4	26.9(7)	33.8(7)	41.9(8)	19.8(6)	1.8(6)	11.6(6)
O2	24.6(7)	30.8(7)	28.4(7)	3.0(5)	1.4(5)	-1.3(6)
O1	30.2(7)	41.5(8)	31.8(7)	16.6(6)	4.1(6)	7.1(6)
O8	39.2(8)	34.4(8)	35.5(7)	-2.8(6)	-8.3(6)	25.9(7)
O7	39.6(8)	42.5(8)	30.4(7)	4.6(6)	-3.3(6)	26.4(7)
O3	24.9(8)	58.1(11)	72.2(12)	43.5(10)	-6.3(8)	-0.1(7)
O5	56.7(11)	48.6(10)	71.2(12)	-26.1(9)	-31.3(9)	39.2(9)
C3	19.7(8)	25.4(8)	22.0(8)	5.4(6)	2.7(6)	9.7(7)
C10	20.6(8)	23.5(8)	20.4(7)	3.1(6)	2.8(6)	10.1(7)
C9'	22.0(8)	28.6(9)	23.2(8)	6.1(6)	3.8(6)	14.4(7)
C9	19.5(8)	24.1(8)	20.6(7)	2.3(6)	2.3(6)	9.5(6)
C1'	23.9(8)	29.8(9)	22.5(8)	3.0(7)	1.1(6)	15.1(7)
C10'	23.7(8)	29.9(9)	21.5(8)	2.0(6)	1.5(6)	14.4(7)
C4	19.8(8)	26.6(9)	26.2(8)	6.5(7)	2.7(6)	9.1(7)
C1	21.2(8)	25.5(8)	21.5(8)	4.5(6)	2.9(6)	10.5(7)
C20	25.5(9)	30.8(9)	25.7(8)	5.3(7)	3.8(7)	16.1(7)
C6	21.4(8)	29.5(9)	21.4(8)	1.5(6)	-0.1(6)	14.3(7)
C2	18.6(7)	27.9(8)	19.2(7)	2.5(6)	0.9(6)	11.9(7)
C8	23.2(8)	24.3(8)	24.6(8)	4.4(6)	1.8(6)	10.6(7)
C11	20.4(8)	28.5(9)	27.2(8)	4.9(7)	1.8(7)	10.7(7)
C6'	20.9(8)	31.8(9)	23.1(8)	3.9(7)	0.5(6)	13.6(7)
C14	24.9(9)	30.9(9)	26.6(9)	9.9(7)	2.8(7)	10.8(8)
C5	19.2(8)	29.1(9)	29.2(9)	5.3(7)	0.8(7)	9.3(7)
C8'	25.5(9)	27.2(9)	27.1(8)	5.6(7)	3.1(7)	13.8(7)
C7'	25.3(9)	28.0(9)	26.8(9)	3.4(7)	0.6(7)	12.5(7)
C7	25.9(9)	30.2(9)	24.1(8)	7.2(7)	2.4(7)	14.7(7)
C2'	23.7(8)	34.5(10)	20.5(8)	-0.8(7)	-2.1(6)	17.3(8)
C3'	25.9(9)	31.0(9)	22.9(8)	-0.7(7)	-1.7(7)	16.3(7)

C4'	28.0(9)	30.3(9)	28.8(9)	-0.4(7)	-2.8(7)	17.0(8)
C17	30.1(10)	35.6(10)	27.6(9)	-1.2(7)	-2.6(7)	19.7(8)
C5'	28.9(9)	33.0(10)	30.4(9)	2.0(7)	-2.3(7)	19.5(8)
C18	31.8(10)	29.7(10)	33.4(10)	-6.1(8)	-0.3(8)	12.4(8)
C12	24.6(9)	26.7(10)	41.6(11)	4.7(8)	4.1(8)	-1.4(7)
C21	39.6(11)	33.7(10)	43.6(11)	1.3(9)	-0.3(9)	25.7(9)
C15	35.4(11)	37.4(11)	45.5(12)	25.8(9)	6.1(9)	13.6(9)
C13	35.2(11)	29.4(10)	43.3(12)	1.6(9)	0.0(9)	6.9(9)
C19	29.6(11)	47.5(13)	42.3(12)	-11.1(10)	-2.9(9)	15.4(10)
C22	52.2(14)	36.3(11)	43.5(12)	-0.8(9)	-3.0(10)	26.7(11)
C16	42.8(13)	50.7(14)	50.8(13)	27.7(11)	9.3(10)	26.5(11)

Table S10. Bond Lengths for **3a**.

Atom	Atom	Length (Å)	Atom	Atom	Length (Å)
C11	C2	1.6738(17)	C9	C8	1.372(2)
C12	C2'	1.6817(18)	C1'	C20	1.443(3)
O6	C17	1.306(2)	C1'	C2'	1.389(2)
O6	C18	1.426(2)	C10'	C3'	1.403(2)
O4	C14	1.308(2)	C10'	C4'	1.368(2)
O4	C15	1.421(2)	C4	C5	1.365(2)
O2	C11	1.317(2)	C1	C2	1.379(2)
O2	C12	1.423(2)	C1	C11	1.445(3)
O1	C11	1.184(2)	C6	C6'	1.478(2)
O8	C20	1.320(2)	C6	C5	1.372(3)
O8	C21	1.429(2)	C6	C7	1.369(3)
O7	C20	1.183(2)	C8	C7	1.368(2)
O3	C14	1.180(2)	C6'	C7'	1.374(3)
O5	C17	1.186(2)	C6'	C5'	1.370(3)
C3	C10	1.400(2)	C8'	C7'	1.364(2)
C3	C2	1.384(2)	C2'	C3'	1.381(2)
C3	C14	1.436(3)	C3'	C17	1.440(3)
C10	C9	1.437(2)	C4'	C5'	1.363(2)
C10	C4	1.366(2)	C18	C19	1.475(3)
C9'	C1'	1.398(2)	C12	C13	1.477(3)
C9'	C10'	1.440(3)	C21	C22	1.470(3)
C9'	C8'	1.376(2)	C15	C16	1.464(3)
C9	C1	1.391(2)			

Table S11. Bond Angles for **3a**.

Atom	Atom	Atom	Angle (°)	Atom	Atom	Atom	Angle (°)
C17	O6	C18	116.59(16)	C3	C2	C11	125.84(14)
C14	O4	C15	116.42(16)	C1	C2	C11	123.86(14)
C11	O2	C12	118.03(16)	C1	C2	C3	110.27(15)
C20	O8	C21	115.34(15)	C7	C8	C9	130.09(18)
C10	C3	C14	124.08(16)	O2	C11	C1	110.89(16)
C2	C3	C10	107.09(16)	O1	C11	O2	124.41(18)
C2	C3	C14	128.83(16)	O1	C11	C1	124.67(17)
C3	C10	C9	107.57(15)	C7'	C6'	C6	117.49(16)
C4	C10	C3	126.11(17)	C5'	C6'	C6	116.41(16)
C4	C10	C9	126.31(16)	C5'	C6'	C7'	126.10(17)
C1'	C9'	C10'	106.88(15)	O4	C14	C3	114.20(16)
C8'	C9'	C1'	126.74(17)	O3	C14	O4	121.71(18)
C8'	C9'	C10'	126.36(16)	O3	C14	C3	124.09(18)
C1	C9	C10	107.00(15)	C4	C5	C6	130.83(18)
C8	C9	C10	127.37(16)	C7'	C8'	C9'	130.40(18)
C8	C9	C1	125.63(17)	C8'	C7'	C6'	129.63(18)
C9'	C1'	C20	128.93(16)	C8	C7	C6	129.28(17)
C2'	C1'	C9'	107.15(16)	C1'	C2'	C12	123.85(14)
C2'	C1'	C20	123.92(16)	C3'	C2'	C12	124.74(14)
C3'	C10'	C9'	108.38(15)	C3'	C2'	C1'	111.39(15)
C4'	C10'	C9'	126.73(16)	C10'	C3'	C17	124.78(17)
C4'	C10'	C3'	124.85(17)	C2'	C3'	C10'	106.19(16)
C5	C4	C10	129.54(18)	C2'	C3'	C17	129.02(16)
C9	C1	C11	124.96(16)	C5'	C4'	C10'	129.66(18)
C2	C1	C9	108.03(16)	O6	C17	C3'	114.29(16)
C2	C1	C11	126.99(16)	O5	C17	O6	121.62(19)
O8	C20	C1'	113.10(15)	O5	C17	C3'	124.07(18)
O7	C20	O8	122.79(17)	C4'	C5'	C6'	130.86(18)
O7	C20	C1'	124.11(17)	O6	C18	C19	107.51(18)
C5	C6	C6'	115.26(16)	O2	C12	C13	106.15(18)
C7	C6	C6'	118.21(16)	O8	C21	C22	106.92(17)
C7	C6	C5	126.53(16)	O4	C15	C16	107.80(18)

Table S12. Torsion angles for **3a**.

A	B	C	D	Angle (°)	A	B	C	D	Angle (°)
C12	C2'	C3'	C10'	-177.69(15)	C2	C3	C10	C9	1.27(19)
C12	C2'	C3'	C17	2.8(3)	C2	C3	C10	C4	-179.00(17)

C3	C10	C9	C1	-1.75(19)	C2	C3	C14	O4	-6.6(3)
C3	C10	C9	C8	178.71(17)	C2	C3	C14	O3	172.8(2)
C3	C10	C4	C5	-177.65(19)	C2	C1	C11	O2	-38.2(3)
C10	C3	C2	C11	-178.22(13)	C2	C1	C11	O1	143.4(2)
C10	C3	C2	C1	-0.3(2)	C8	C9	C1	C2	-178.90(17)
C10	C3	C14	O4	173.50(17)	C8	C9	C1	C11	2.4(3)
C10	C3	C14	O3	-7.2(3)	C11	O2	C12	C13	164.69(18)
C10	C9	C1	C2	1.56(19)	C11	C1	C2	C11	-4.2(3)
C10	C9	C1	C11	-177.14(16)	C11	C1	C2	C3	177.86(17)
C10	C9	C8	C7	-0.8(3)	C6'	C6	C5	C4	176.97(19)
C10	C4	C5	C6	-0.1(4)	C6'	C6	C7	C8	-177.36(18)
C9'	C1'	C20	O8	-15.9(3)	C14	O4	C15	C16	176.6(2)
C9'	C1'	C20	O7	164.2(2)	C14	C3	C10	C9	-178.81(16)
C9'	C1'	C2'	C12	177.79(14)	C14	C3	C10	C4	0.9(3)
C9'	C1'	C2'	C3'	-0.9(2)	C14	C3	C2	C11	1.9(3)
C9'	C10'	C3'	C2'	-0.7(2)	C14	C3	C2	C1	179.77(18)
C9'	C10'	C3'	C17	178.83(18)	C5	C6	C6'	C7'	131.49(19)
C9'	C10'	C4'	C5'	1.2(4)	C5	C6	C6'	C5'	-48.1(2)
C9'	C8'	C7'	C6'	0.3(4)	C5	C6	C7	C8	1.9(3)
C9	C10	C4	C5	2.0(3)	C8'	C9'	C1'	C20	-1.5(3)
C9	C1	C2	C11	177.16(13)	C8'	C9'	C1'	C2'	178.79(18)
C9	C1	C2	C3	-0.8(2)	C8'	C9'	C10'	C3'	-178.18(18)
C9	C1	C11	O2	140.24(18)	C8'	C9'	C10'	C4'	3.8(3)
C9	C1	C11	O1	-38.1(3)	C7'	C6'	C5'	C4'	-1.6(4)
C9	C8	C7	C6	0.3(3)	C7	C6	C6'	C7'	-49.2(2)
C1'	C9'	C10'	C3'	0.2(2)	C7	C6	C6'	C5'	131.22(19)
C1'	C9'	C10'	C4'	-177.86(19)	C7	C6	C5	C4	-2.3(3)
C1'	C9'	C8'	C7'	176.8(2)	C2'	C1'	C20	O8	163.84(18)
C1'	C2'	C3'	C10'	1.0(2)	C2'	C1'	C20	O7	-16.0(3)
C1'	C2'	C3'	C17	-178.5(2)	C2'	C3'	C17	O6	-7.5(3)
C10'	C9'	C1'	C20	-179.78(18)	C2'	C3'	C17	O5	170.7(2)
C10'	C9'	C1'	C2'	0.5(2)	C3'	C10'	C4'	C5'	-176.5(2)
C10'	C9'	C8'	C7'	-5.1(3)	C4'	C10'	C3'	C2'	177.35(19)
C10'	C3'	C17	O6	173.09(18)	C4'	C10'	C3'	C17	-3.1(3)
C10'	C3'	C17	O5	-8.7(4)	C17	O6	C18	C19	-172.87(19)
C10'	C4'	C5'	C6'	-2.4(4)	C5'	C6'	C7'	C8'	3.8(3)
C4	C10	C9	C1	178.51(17)	C18	O6	C17	O5	0.6(3)
C4	C10	C9	C8	-1.0(3)	C18	O6	C17	C3'	178.81(18)
C1	C9	C8	C7	179.71(18)	C12	O2	C11	O1	-7.7(3)
C20	O8	C21	C22	-172.2(2)	C12	O2	C11	C1	173.93(17)
C20	C1'	C2'	C12	-2.0(3)	C21	O8	C20	O7	1.5(3)

C20	C1'	C2'	C3'	179.28(17)	C21	O8	C20	C1'	-178.34(17)
C6	C6'	C7'	C8'	-175.81(19)	C15	O4	C14	O3	3.7(3)
C6	C6'	C5'	C4'	178.0(2)	C15	O4	C14	C3	-176.95(18)

Table S13. Hydrogen Atom Coordinates ($\text{\AA} \times 10^4$) and Isotropic Displacement Parameters ($\text{\AA}^2 \times 10^3$) for **3a**.

Atom	<i>x</i>	<i>y</i>	<i>z</i>	U(eq)
H4	8083.72	1971.73	9203.09	31
H8	11465.52	6470.39	8215.23	30
H5	6508.64	2053.13	8059.23	33
H8'	4917.46	5435.67	6226.19	32
H7'	6858.68	5496.67	7165.78	34
H7	9195.17	5631.57	7257.96	32
H4'	4004.4	407.04	5387.54	36
H5'	6067.13	1455.61	6530.02	37
H18A	-865.64	-3121.87	3514.65	42
H18B	118.59	-2565.2	2753.78	42
H12A	16045.11	9665.68	10042.01	45
H12B	17009.56	8852.14	10345.32	45
H21A	1562.86	6593.25	5816.74	45
H21B	2728.21	7262.33	5157.47	45
H15A	10616.06	185.21	11030.85	48
H15B	10434.97	1113.52	11879.94	48
H13A	15870.31	10162.98	11547.97	62
H13B	17679.04	10759.15	11560.44	62
H13C	16698.87	9249.54	11864.78	62
H19A	-1827.47	-2253.42	1923.49	67
H19B	-2775.27	-2642.44	2710.89	67
H19C	-2621.16	-3883.77	2097.53	67
H22A	4856.7	8417.18	6415.96	67
H22B	3774.34	7653.63	7091.11	67
H22C	3585.38	8861.45	6616.12	67
H16A	13310.24	1311.52	11712.30	68
H16B	12289.61	406.56	12373.48	68
H16C	13070.83	2151.39	12574.48	68

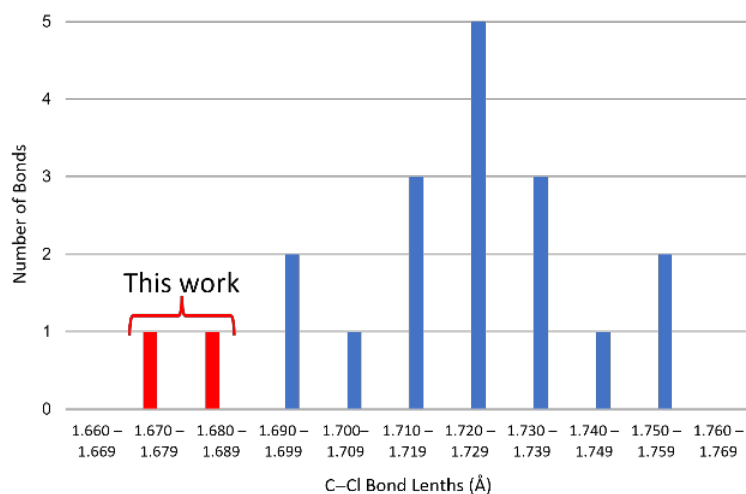
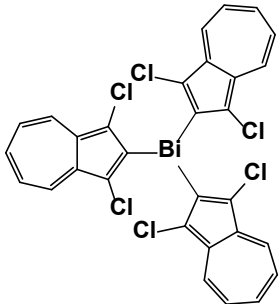
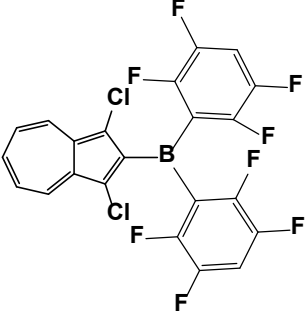
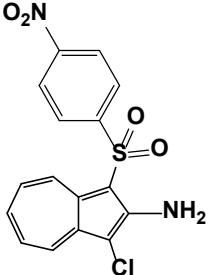
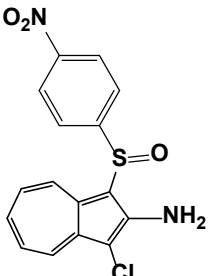
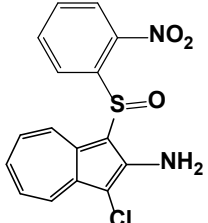
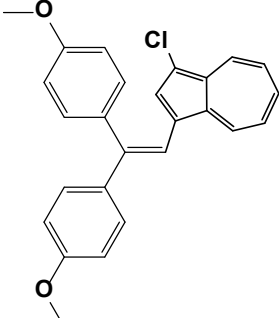


Figure S22. Distribution of the C–Cl bond distances for chloroazulenes featuring Cl-substitution at the five-membered ring of their azulenic scaffold: this work plus 17 hits (Table S14) in CCDC, version 5.45 (Nov. 2023), accessed on Nov. 15, 2023.

Table S14. X-ray crystallographically characterized chloroazulenes represented in Fig. S22.

Molecular structure	$d(\text{C}^2\text{-Cl})$, Å	CCDC identifier
	1.674(2) 1.682(2)	This work
	1.7117 (17)	HOMRAE
	1.709(2)	AYIDIX
	1.714(4)	XIGPOU
	1.71(2) 1.72(2)	FAQGUA

	<p>1.75(2) 1.75(2) 1.69(2) 1.69(2) 1.74(2) 1.73(2)</p>	<p>FAQGOU</p>
	<p>1.7237(17) 1.7234(17)</p>	<p>UROCAI</p>
	<p>1.722(4)</p>	<p>XOWQAD</p>
	<p>1.730(2)</p>	<p>XOWQEH</p>
	<p>1.726(3)</p>	<p>XOXCOE</p>

	1.732(3)	EZITEM
---	----------	--------

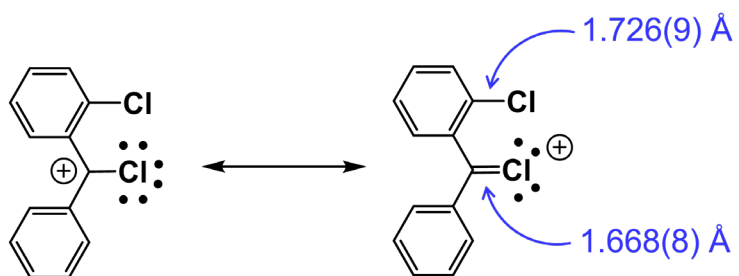


Figure S23. The chlorodiphenylmethyl cation X-ray crystallographically characterized by Laube et al.²⁰

References

- (1) T.R. Maher, A.D. Spaeth, B.M. Neal, C.L. Berrie, W.H. Thompson, V.W. Day and M.V. Barybin, *J. Am. Chem. Soc.*, 2010, **132**, 15924-15926.
- (2) P.T. Connelly, J.C. Applegate, D.A. Maldonado, M.K. Okeowo, W.C. Henke, A.G. Oliver, C.L. Berrie and M.V. Barybin, *Dalton Trans.*, 2023, **52**, 11419-11426.
- (3) M. Makosza, P. W. Osinski, and S. Ostrowski, *Pol. J. Chem.*, 2001, **75**, 275-281.
- (4) I. Suzuka and M. Yasunami, Japan JP2008285435, 2008.
- (5) T. Nozoe, S. Seto and S. Matsumura, *Bull. Chem. Soc. Jpn.*, 1962, **35**, 1990-1998.
- (6) D.L. DuBose, R.E. Robinson, T.C. Holovics, D.R. Moody, E.C. Weintrob, C.L. Berrie, and M.V. Barybin, *Langmuir*, 2006, **22**, 4599-4606.
- (7) S. Ito, T. Okujima and N. Morita, *J. Chem. Soc., Perkin Trans. 1*, 2002, **16**, 1896-1905.
- (8) B. Hou, Z. Zhou, C. Yu, X.-S. Xue, J. Zhang, X. Yang, J. Li, C. Ge, J. Wang and X. Gao, *ACS Macro Lett.*, 2022, **11**, 680-686.
- (9) H. Xin, C. Ge, X. Yang, H. Gao, X. Yang and X. Gao, *Chem. Sci.*, 2016, **7**, 6701-6705.
- (10) K. Kurotobi, H. Tabata, M. Miyauchi, T. Murafuji and Y. Sugihara, *Synthesis*, 2002, **8**, 1013-1016.
- (11) E. Epifanovsky *et al.*, *J. Chem. Phys.*, 2021, **155**, 084801.
- (12) A.D. Becke, *J. Chem. Phys.*, 1993, **98**, 5648-5652.
- (13) T.H. Dunning Jr., *J. Chem. Phys.* 1989, **90**, 1007-1023.
- (14) E. Cancès, B. Mennucci and J. Tomasi, *J. Chem. Phys.*, 1997, **107**, 3032-3041.
- (15) Q. Wu and T. Van Voorhis, *J. Chem. Theory Comput.*, 2006, **2**, 765-777.
- (16) Rigaku Oxford Diffraction (2022). CrysAlis PRO. Rigaku Oxford Diffraction, Tokyo, Japan.
- (17) O.V. Dolomanov, L.J. Bourhis, R.J. Gildea, J.A.K. Howard and H.J. Puschmann, *Appl. Cryst.* 2009, **42**, 339-341.
- (18) G.M. Sheldrick, *Acta Cryst.*, 2015, **A71**, 3-8.
- (19) G.M. Sheldrick, *Acta Cryst.*, 2015, **C71**, 3-8.
- (20) T. Laube, E. Bannwart, and S. Hollenstein, *J. Am. Chem. Soc.*, 1993, **115**, 1731-1733.